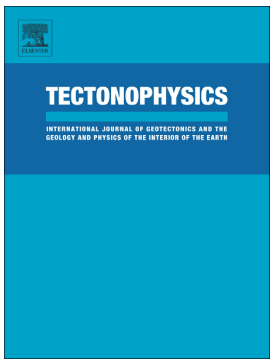

Miocene deformation in the orogenic front of the Malargüe fold-and-thrust belt (35°30′–36° S): Controls on the migration of magmatic and hydrocarbon fluids

M. Barrionuevo, L. Giambiagi, J. Mescua, J. Suriano, H. de la Cal, J.L. Soto, A.C. Lossada

PII: S0040-1951(19)30236-7
DOI: https://doi.org/10.1016/j.tecto.2019.06.005
Reference: TECTO 128135

To appear in: *Tectonophysics*

Received date: 15 January 2019
Revised date: 31 May 2019
Accepted date: 8 June 2019

Please cite this article as: M. Barrionuevo, L. Giambiagi, J. Mescua, et al., Miocene deformation in the orogenic front of the Malargüe fold-and-thrust belt (35°30′–36° S): Controls on the migration of magmatic and hydrocarbon fluids, Tectonophysics, https://doi.org/10.1016/j.tecto.2019.06.005

Miocene deformation in the orogenic front of the Malargüe fold-and-thrust belt (35º30'-36° S): controls on the migration of magmatic and hydrocarbon fluids

M. Barrionuevo [1], L. Giambiagi [1], J. Mescua [1,2], J. Suriano [1], H. de la Cal [3], J. L. Soto [3], A. C. Lossada[4]

1. Instituto Argentino de Nivología, Glaciología y Ciencias Ambientales (IANIGLA), CCT Mendoza, CONICET, Argentina
2. Facultad de Ciencias Exactas y Naturales, Universidad Nacional de Cuyo, Argentina
3. Roch S.A., Argentina
4. Instituto de Estudios Andinos (IDEAN), Universidad de Buenos Aires, CONICET, Buenos Aires, Argentina

Corresponding author: Matías Barrionuevo. mbarrionuevo@mendoza-conicet.gob.ar / matbarrionuevo@yahoo.com.ar. Av. Ruiz Leal s/n Parque General San Martín, CP 5500-CC 330. Mendoza, Argentina.

Abstract

The integration of surface observations and sub-surface data (wellbore and seismic) from the orogenic front of the Malargüe fold-and-thrust belt allows us to study its structural kinematics, and to interpret the local stress field and its control over fluid (magmatic and hydrocarbon) migration. Reverse faults correspond to inverted NNW-striking Mesozoic normal faults and N-S striking Cenozoic low-angle thrusts parallel to the orogen. Oblique structures with strike-slip movement are also present. The magmatic activity in the study area was strongly controlled by this structural framework and the in-situ stress field. Miocene dykes and sills were emplaced in relation to strike-slip and reverse faults, respectively. We propose an evolution of the study region from a foredeep sector, in the early-middle Miocene, to a peak in deformation in the late Miocene, and finally a waning of deformation

from the Pliocene to the present. Our structural model suggests that during the evolution of the thrust front, the in-situ stress field changed from a compressional to strike-slip/compressional stress field, favouring the synchronous emplacement of sills and dykes. This alternation of stress regimes favours hydrocarbon migration through both thrusts and subvertical strike-slip faults. This exchange between both stress regimes is likely related to the similar values of the minimum (σ3) and intermediate (σ2) principal stress with an E-W oriented maximum principal stress (σ1) according to the plate convergence vector.

Keywords: stress field; Southern Central Andes; fluid migration; Neuquén basin; fault reactivation; magma migration

1. Introduction

Fluid migration in fold-and-thrust belts is a complex process with implications for magmatic activity and the emplacement of mineral resources, including economic mineralization and hydrocarbon deposits (Aydin, 2000; Haney et al., 2005; Cox, 2005). The development of fluid migration paths is closely linked to active faults and open fractures, in turn, controlled by the stress conditions (Barton et al., 1995).

The Southern Central Andes provide a natural laboratory for the study of fault reactivation and its relationship with fluid migration during the ongoing migration of the foreland fold-and-thrust belts, due to the combination of inherited pre-Andean structures, magmatic arc activity and the development of the Mesozoic Neuquén basin where one of the main hydrocarbon systems in Argentina is located (Boll et al., 2014, and references therein).

The Malargüe fold-and-thrust belt (Fig. 1) extends between 34º and 36ºS in the normal subduction (i.e. steeper subduction angle compared to subhorizontal or flat-slab zone) segment of the Southern Central Andes, where the Nazca plate subducts beneath the South American plate with an angle of 30° (Barazangi and Isacks, 1976). This area was part of the Neuquén basin, an extensional retroarc basin developed during the Mesozoic (Uliana and

Legarreta, 1993). The initial setup of the basin consisted on normal fault-bounded depocenters developed as a result of extension from the Late Triassic to the Early Jurassic (Vergani et al., 1995) during the synrift stage (Fig. 2). These depocenters, filled with clastic, volcaniclastic and volcanic deposits, were initially isolated and were linked as the extension progressed (Manceda and Figueroa, 1995). The master faults that bounded the depocenters have different polarities and orientations, with NNW and NNE strikes (Giambiagi et al., 2009a).

The Malargüe fold-and-thrust belt has a basement-involved structural style (Kozlowski et al., 1993; Manceda and Figueroa, 1995; Giampaoli et al., 2002; Silvestro et al., 2005, Giambiagi et al., 2009b; Silvestro and Atencio, 2009; Turienzo et al., 2012). Different structural models have been proposed, some related to inversion of Mesozoic normal faults (Manceda and Figueroa 1995; Uliana et al., 1995; among others), others to the development of new thrusts during Andean contraction (Dimieri, 1997; Turienzo, 2010), and finally “hybrid” models which include both inversion and new faults (Yagupsky et al., 2008; Giambiagi et al., 2009b; Orts et al., 2012; Mescua et al., 2014; Branellec et al. 2015a, 2016; Fuentes et al., 2016; Seoane Borracer et al., 2018; Granado & Ruh, 2019).

Here we present the results from a structural study in the orogenic front of the Southern Central Andes, between 35º30’ and 36ºS, where the Andean orogeny was superimposed to the previous structures developed during the opening of the Mesozoic Neuquén basin. We focus our analysis in the Agua Botada oil field (Fig. 1), where we integrate surface and subsurface information into a 3D structural model.

From these observations, we address the subject of: (i) the tectonic inversion of pre-existing faults, (ii) the control by the local stress field and active structures over the emplacement of sills and dykes and over fluid migration, and (iii) how this control varies during the advance of the thrust front.

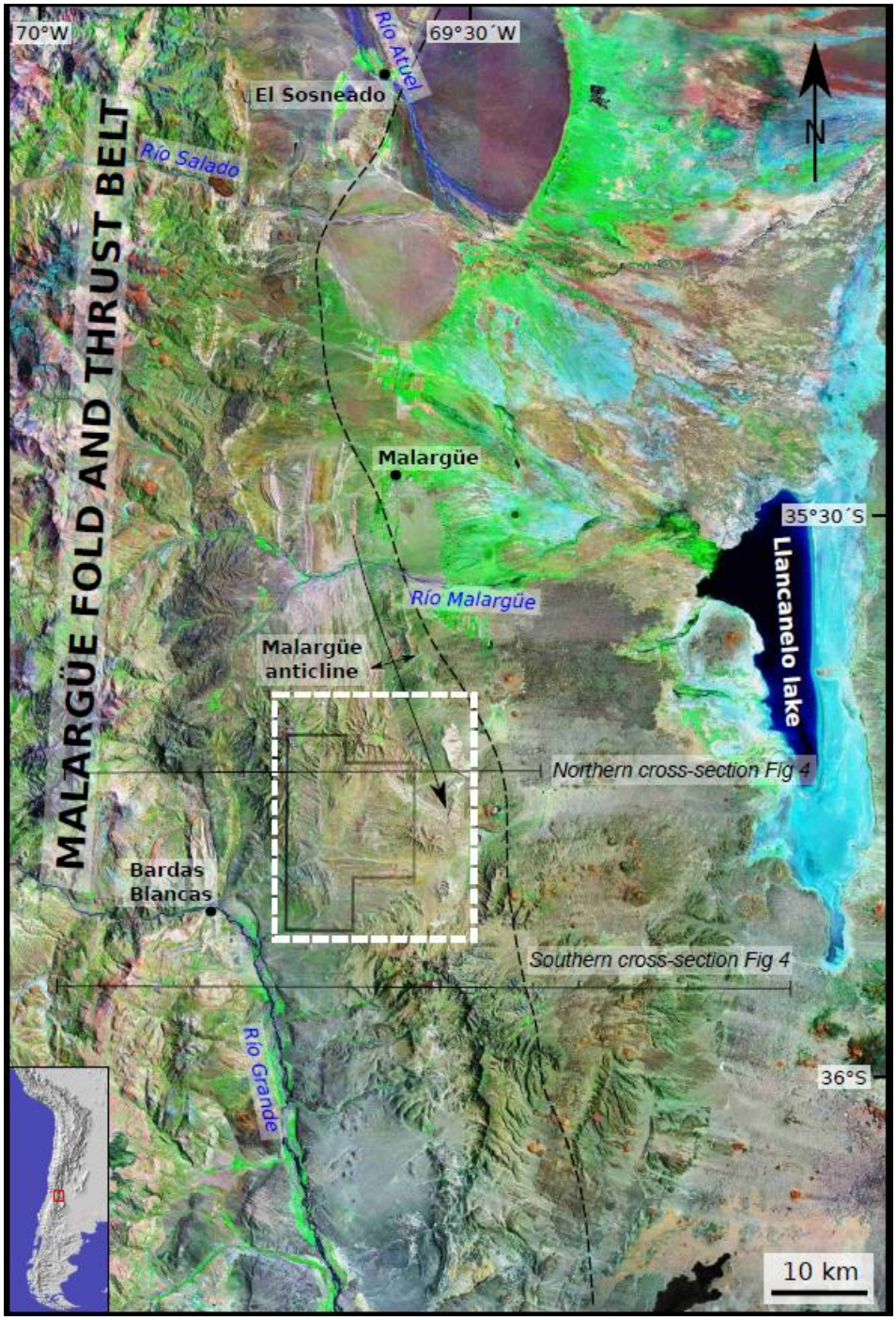

Figure 1: Location of the study area (white dashed rectangle) including the Agua Botada oil field (black continue polygon) and surroundings, with indication of the regional balanced cross-sections shown in Fig. 4. Base image is a LANDSAT7+ satellite image (RGB741 band combination).

2. Geological setting

2.1 The northern Neuquén basin

During the Late Triassic to Early Jurassic, extension along the western South American continental margin resulted in the opening of the Neuquén basin (Uliana et al., 1989; Vergani et al., 1995; Franzese and Spalletti, 2001). The basement of this basin, composed mainly of Permian to Triassic volcanic and plutonic rocks of the Choiyoi Group, was affected by structures inherited from previous tectonic stages (Mosquera and Ramos, 2006; Kleiman and Japas, 2009; Bechis et al., 2014). Northeast of the study area, structures related to the Permian San Rafael orogeny are NNW- to NW-striking faults (Kleiman and Japas, 2009).

The Agua Botada area (Figs. 1, 2) is located in the northern part of this oil-bearing basin, which presents an almost continuous record of up to 7,000 m of Late Triassic to Paleocene marine and continental deposits representing different tectonic scenarios from a backarc extensional basin followed by a postextensional setting and finally a retroarc foreland basin (Fig. 3, Uliana et al., 1989; Legarreta and Gulisano, 1989; Vergani et al., 1995; Legarreta and Uliana, 1999). In this part, the basin is composed of several NNE- to NNW-trending depocenters, which are from north to south: Atuel, Malargüe, Valenciana, Río del Cobre, Palauco and Sierra Azul (Fig. 2B). The Agua Botada oil field (Figs.1, 2) is located between the Malargüe and Palauco depocenters (Fig. 2C).

The Malargüe depocenter developed at the beginning of extension in the Neuquén basin, affecting the basement, and it is filled with synrift clastic and volcaniclastic, braided-river plain deposits interbedded with lacustrine black shales grouped in the Upper Triassic-Lower Jurassic Pre-Cuyo Cycle (Fig.3, Spalletti, 1997; Artabe et al., 1998; Buchanan et al., 2017). The depocenter was controlled by a NNW-striking, west dipping, master fault called Malargüe fault (Manceda and Figueroa, 1995; Silvestro et al., 2005; Giambiagi et al., 2009a; Fig. 2B).

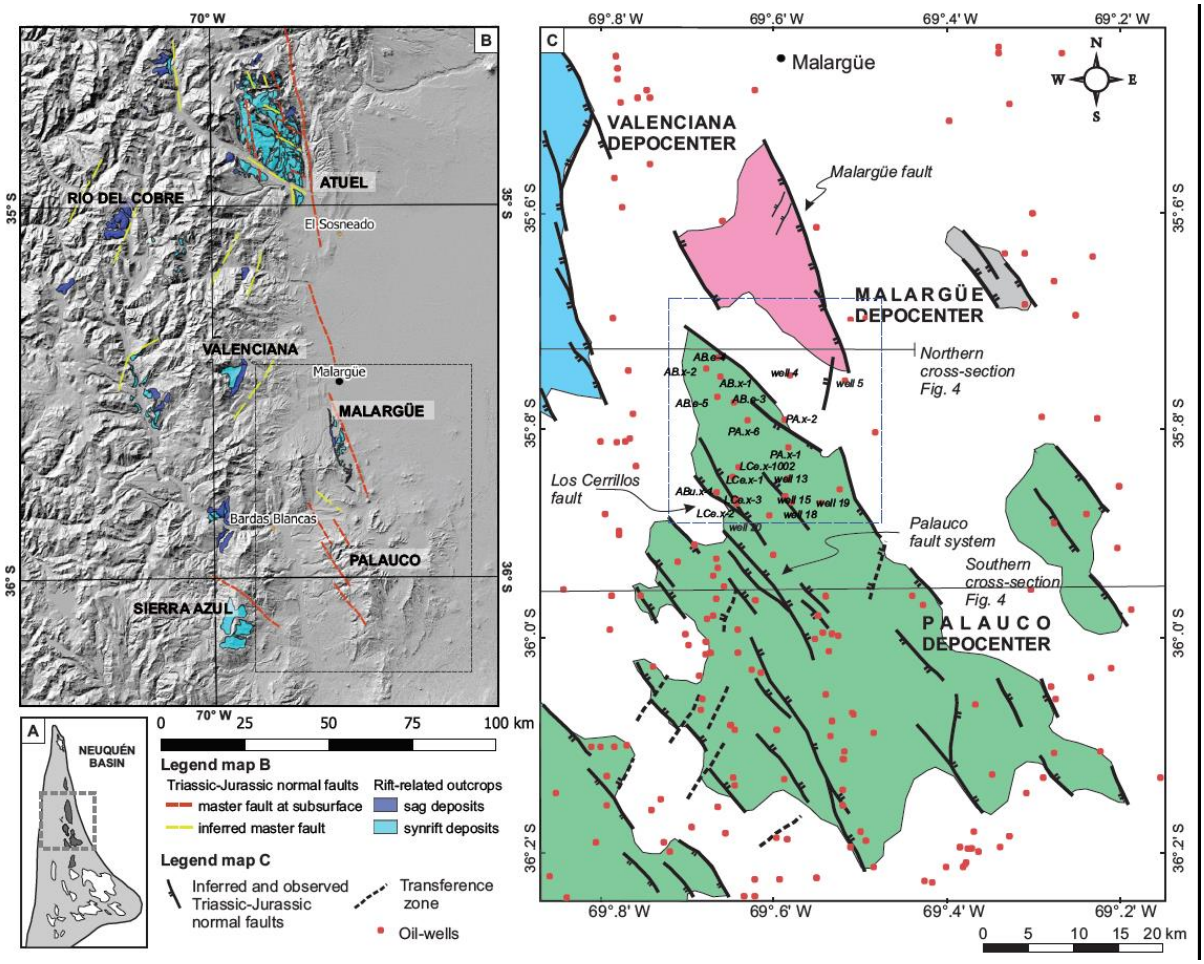

Figure 2: A) Areal extension of the Neuquén basin (grey square shows the location of fig 2B). B) Map showing the master faults that bounded the Atuel, Río del Cobre, Valenciana, Malargüe, Palauco and Sierra Azul depocenters) of the Neuquén basin with indication of rift-related deposits (modified from Bechis et al., in press). C) Detailed map of the Valenciana (light blue area), Malargüe (pink area) and Palauco (green area) depocenters with the distribution of the Upper Triassic-Lower Jurassic synrift deposits and the main normal faults inferred from subsurface and surface data. The Agua Botada area corresponds to the blue dashed rectangle between Malargüe and Palauco depocenters (modified from Giambiagi et al., 2009a).

The Palauco depocenter is filled up with volcaniclastic deposits of the Upper Triassic-Lower Jurassic Pre-Cuyo Cycle (Fig. 3, Gulisano, 1981; Legarreta and Gulisano, 1989) and it is

affected by two master faults controlling the accommodation space, the NNW-striking, ENE-dipping, previously proposed Palauco fault (Manceda and Figueroa, 1995; Giambiagi et al., 2009a) and the Los Cerrillos fault (Fig. 2C).

These previously isolated depocenters were linked during the Middle Jurassic sag phase (Uliana and Biddle, 1988; Uliana and Legarreta, 1993; Vergani et al., 1995). During the Middle Jurassic and Early Cretaceous a thick pile of evaporitic, calcareous and clastic marine and continental sedimentary rocks belonging to the Cuyo, Lotena, Mendoza and Rayoso Groups were deposited (Fig. 3). A brief episode of extension occurred during the deposition of the Upper Jurassic Tordillo Formation red sandstones at this latitude, subsequently followed by another sag stage during the Early Cretaceous (Fig. 3, Mescua et al., 2014). In the Late Cretaceous, coarse continental deposits belonging to the Neuquén Group (Uliana and Legarreta, 1993; Vergani et al., 1995) represent the foreland basin stage related to the beginning of the Andean shortening.

The Oxfordian Auquilco and Aptian-Albian Huitrín anhydrite units (Fig. 3) are the main detachment levels for thin-skinned thrust sheets (Kozlowski et al., 1993), and also act as seals for hydrocarbon accumulations (Cobbold and Rossello, 2003). The Neocomian black shales of the Vaca Muerta Formation, which are the main source-rock of the basin, are also an important detachment level for thrusts (Kozlowski et al., 1993).

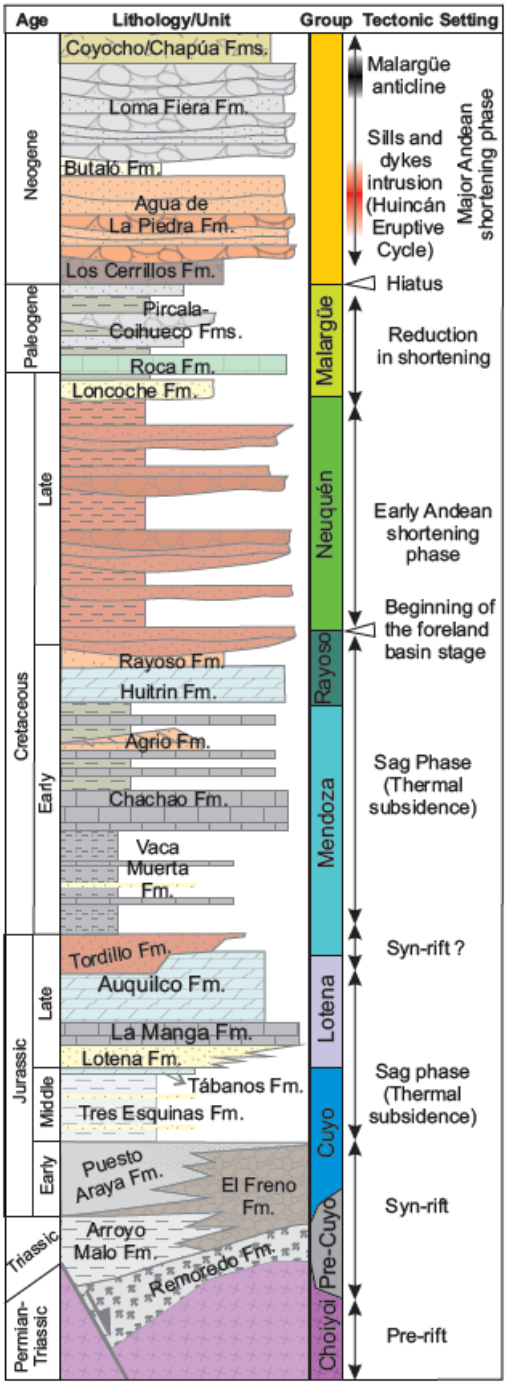

Figure 3: Stratigraphic chart showing the main tectonic phases of the Neuquén Basin and Malargüe fold-and-thrust belt (based on Giampaoli et al., 2002; Giambiagi et al., 2008; Mescua et al., 2014; Horton et al., 2016).

2.2. The Malargüe fold and thrust belt

Deformation of the Malargüe fold-and-thrust belt started in the Late Cretaceous in its western sector (Tunik et al., 2010; Mescua et al., 2013; Balgord and Carrapa, 2016; Fennell et al., 2017). The study area is located in the foredeep sector of the Cretaceous foreland basin, filled with up to 1.5 km thick continental fluvial deposits of the Neuquén Group (Uliana and Legarreta, 1993; Balgord and Carrapa, 2016). The sedimentation rate diminished during the deposition of mudstones and sandstones of the Malargüe Group in the Paleocene-Eocene, probably due to the cessation or reduction in shortening (Legarreta and Gulisano, 1989; Horton et al., 2016), followed by a non-deposition period with a stratigraphical hiatus spanning between 40 and 20 Ma (Horton et al., 2016).

Shortening and uplift resumed in the middle to late Miocene (Giambiagi et al., 2003a, b, 2008, 2015; Spagnuolo et al., 2012; Orts et al., 2012, Boll et al., 2014; Fuentes et al., 2016; Horton et al., 2016). During this Miocene shortening phase, predominantly N-striking basement thrusts and reverse faults were active and transferred shortening to the Neuquén basin cover (Manceda and Figueroa, 1995; Uliana et al., 1995; Zapata et al., 1999; Giambiagi et al., 2003b, 2008). The foreland basin related to this orogenic event was filled with 1.5-2 km-thick, clastic rocks of the Agua de la Piedra and Butaló Formations (approx. 16-10 Ma; Silvestro and Atencio, 2009) and volcaniclastic successions of the Loma Fiera Formation (approx. 11-8 Ma; Silvestro and Atencio, 2009). In the northern sector of the study area, a forelandward progression of the deformation has been determined, with deformation at the orogenic front represented by the Malargüe anticline (Figs. 4, 5) since 8-7 Ma (Silvestro et al., 2005). In contrast, in the southern part of the study area, the easternmost structures of the Sierra the Palauco (Fig. 4) were uplifted early in the history of the belt (17 Ma, Silvestro and Atencio, 2009) and experienced a reactivation phase between 11-8 Ma, as recorded by angular unconformities in the synorogenic volcaniclastic deposits (Silvestro and Atencio, 2009).

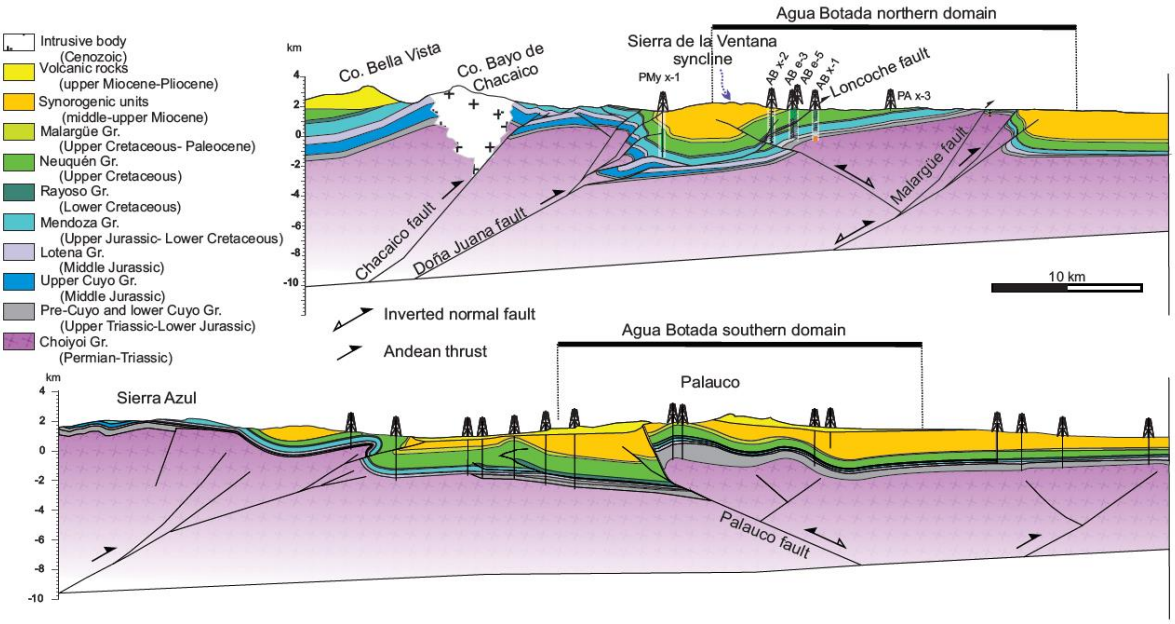

Figure 4

Figure 4: Regional balanced cross-sections, modified from Giambiagi et al. (2009b). See location in figure 1. The northern section cuts the Agua Botada northern domain. In this domain, the Malargüe fault (and fault-related anticline) is the main basement structure. The southern section crosses close to (~5 km) the Agua Botada southern domain, characterized by the inversion of a Triassic-Jurassic normal fault, the Palauco west-directed fault.

Furthermore, the northern and southern sectors are also differentiated by the vergence of the main structures (Fig. 4). The northern and southern sectors are characterized by eastern and western vergence, respectively, which seems to indicate that the Andean structure has been significantly controlled by the inherited geometry of the Late Triassic to Early Jurassic Neuquén extensional basin (Fig. 2C).

Active (Pliocene-recent) N-striking reverse faults and oblique strike-slip faults (Spacapan et al., 2016; Stein et al., 2018; Mescua et al., in review) are documented in the orogenic front of the Malargüe fold-and-thrust belt.

2.3. Magmatic activity

The magmatic activity in the eastern Malargüe fold-and-thrust belt has been separated into two cycles: the late Oligocene to middle Miocene Molle Eruptive Cycle and the middle Miocene to Pliocene Huincán Eruptive Cycle (Fig. 3). The first one associated with retroarc volcanism and the latter to arc volcanism (Groeber, 1946; Bettini, 1982; Baldauf, 1997; Nullo et al., 2002; Sruoga et al., 2009; Combina and Nullo, 2011; Litvak et al., 2015). Both cycles correspond to predominantly basaltic and andesitic magmatism, represented by many lava flow sequences and subvolcanic bodies such as sills, dykes and laccoliths (Baldauf, 1997; Combina and Nullo, 2011; Spacapan et al., 2016, 2017). The Coyocho Basalt (Fig. 3), corresponding to the final part of the Huincán Cycle (6.7 to 2.3 Ma, Silvestro and Atencio, 2009), unconformably covers the deformed Neogene strata, outcropping mainly to the west of our study area. The youngest volcanism is located towards the east, in the Quaternary Payenia Basaltic Province (Bermúdez et al., 1993; Ramos and Folguera, 2011).

The Neogene intrusives emplaced in the Mesozoic source rocks are one of the main fractured reservoirs in the hydrocarbon fields in this sector of the basin (Schiuma, 1994; Rodriguez Monreal et al., 2009; Witte et al., 2012; Schiuma and Llambias, 2014; Spacapan et al., 2018). Furthermore, the source rock maturation due to the thermal impact of these intrusives in the Río Grande area, south of Agua Botada, was modelled by Spacapan et al. (2018) suggesting that two pulses of hydrocarbon generation were triggered by the two magmatic cycles mentioned above.

In the Agua Botada sector, Cenozoic intrusives correspond to sills, subvolcanic bodies and dykes with predominantly intermediate compositions (Schiuma, 1994). Available K/Ar ages on dykes in the study area provided early to middle Miocene ages (17.3±0.8 and 14.4±0.7 Ma, Valencio et al., 1969).

Andesitic and basaltic andesite sills are predominantly emplaced in units with fine grained intervals within the study area, particularly in the black shales of the Vaca Muerta and Agrio Formations (Schiuma, 1994; Rodriguez Monreal et al., 2009; Spacapan et al., 2016a, 2018). Scapacan et al. (2016a) studied the mechanism of intrusion of sills in this area, based on detailed observations at Cuesta del Chihuido (Fig. 5). They propose a two-stage intrusion

history, where magma fingers push away the host rock in the initial stage, followed by brittle and ductile inelastic deformation of the strata as the sill propagates. Their results are in agreement with the viscous indenter model (Donadieu and Merle, 1998; Mathieu et al., 2008), and underscore the role of strength contrast between thin and thick layers in the Agrio Formation with intrusions confined to the thin and weak layers.

Miocene to Quaternary andesitic and basaltic subvertical dykes are abundant in the easternmost Malargüe fold-and-thrust belt and in the Payenia volcanic province developed to the east, where volcano alignments of several tens of kms are interpreted as the surface expression of dykes in depth (Bermúdez and Delpino, 1989; Spacapan et al., 2016b). The most common orientation of dykes is NW; based on this, igneous intrusion in the area has been interpreted as controlled by the presence of pre-existing NW-striking Paleozoic lineaments (Bermúdez and Delpino, 1989; Llambías et al., 2010; Spacapan et al., 2016b), namely strike-slip faults observed in the basement north of the study area (e.g. Kleiman and Japas, 2009). A secondary E-W dyke trend has been interpreted as opening parallel to the maximum horizontal stress (Hernando et al., 2014; Scapacan et al., 2016b). Two of the NW-trending dykes within our study area, at Cuesta del Chihuido, were studied in detail by Spacapan et al. (2016b). The observations made by these authors underscore the association of the dykes with strike-slip faults, which they interpret as pre-existing structures without activity during or after dyke emplacement. We will discuss this interpretation in the light of our own observations below.

3. Methods

Our methodology consists of structural mapping of the Agua Botada area (Figs. 1, 2) based on fieldwork and satellite image interpretation, structural interpretation of 3D seismic data, analysis of oil-well logs, and collection of fault-slip kinematic data. All the data were integrated into a structural model, based on previous chronological constraints (Silvestro and Atencio, 2009, Arcila Gallego, 2010), results of the kinematic analysis of fault-slip data,

balanced cross-section forward modelling, pseudo-3D structural model construction, and interpretation of Miocene to Quaternary *in-situ* stress fields.

Wellbore data available for the study area (Fig. 5) was analysed to determine thickness variations of units and to locate faults.

Newly acquired 3D seismic data was provided by the company ROCH SA. The seismic vibroseis survey was carried out in 2017 covering 107 km^2 with a bin size of 25 m x 25 m. The source-point intervals were of 50 m and source line distances of 400 m oriented N-S while the receiver array consisted of W-E oriented lines spaced at 400 m each with receiver point intervals of 50 m; this results in a nominal fold of 64. In each vibrator point (VP) three vibroseis were placed and the source density was 50 VP/km^2. The data was migrated through pre-stack time migration.

This 3D seismic data was interpreted using the free software OpendTect 6.4.2. Formation tops recognized in wellbore data were used to pick reflectors and trace unit contacts in the subsurface. The main faults were recognized in the seismic data through the structural interpretation of 2D lines and time slices. Finally, we interpolated these lines to create 3D surfaces which provided us the structural array of the area as a constraint for the kinematic modelling. The combination of fault geometries, thickness variations and stratal geometry of the Late Triassic-Early Jurassic synrift units was used to differentiate reactivated pre-Andean faults and Andean thrusts in the structural model.

Selected cross-sections were forward-modelled using 2D area-balancing techniques with the algorithms provided by MOVE© to obtain the best geometric match between the natural example and the model. Fault-parallel-flow, inclined shear or trishear were used depending on the geometry of the fold-related-fault. The nine cross-sections were the base for the construction of a pseudo-3D model, built using the interpolation tools available in the MOVE© software.

During fieldwork, the orientation of dykes and sills was measured, and their relationship with structures assessed. Fault-slip data of outcrop-scale faults affecting the intrusions were obtained from the measurement of mineral fibers on fault planes, Riedel structures, and

lineations coupled with marker bed displacements. In addition, Google Earth satellite images were used to determine the orientations and length of dykes.

Fault-slip data was analysed using the FaultKinWin software (Allmendinger et al., 2012). This program determines shortening and extension axes for each fault datum and uses Linked Bingham statistics to define the main deformation axes for the whole fault population.

4. Results

4.1 Surface structural mapping

The Agua Botada area (Fig. 5) is located in the backlimb of the Malargüe anticline, a fault-related fold interpreted as the result of the inversion of a Mesozoic normal fault (Silvestro and Atencio, 2009; Giambiagi et al., 2009b; Branellec et al., 2016). This fault was bounding the Malargüe depocenter during the Late Triassic (Manceda and Figueroa, 1995). Fault inversion took place in the late Miocene (7 Ma to recent, Silvestro et al., 2005) with positive reactivation of the lower reaches of the listric normal fault and the development of a short-cut fault in the steeply-dipping upper reaches of the fault (Giambiagi et al., 2009b). The NNW-striking anticline is an asymmetric fold with a steep to overturned forelimb and a subdued backlimb. Basement rocks of the Permian-Triassic Choiyoi Group are exposed in the core of this structure; while to the west, in the backlimb, Upper Triassic to Upper Cretaceous sedimentary and volcaniclastic deposits corresponding to the Pre-Cuyo, Cuyo, Mendoza, Rayoso and Neuquén Groups are cropping out and gently-dipping (i.e., 10º-20º) to the west .

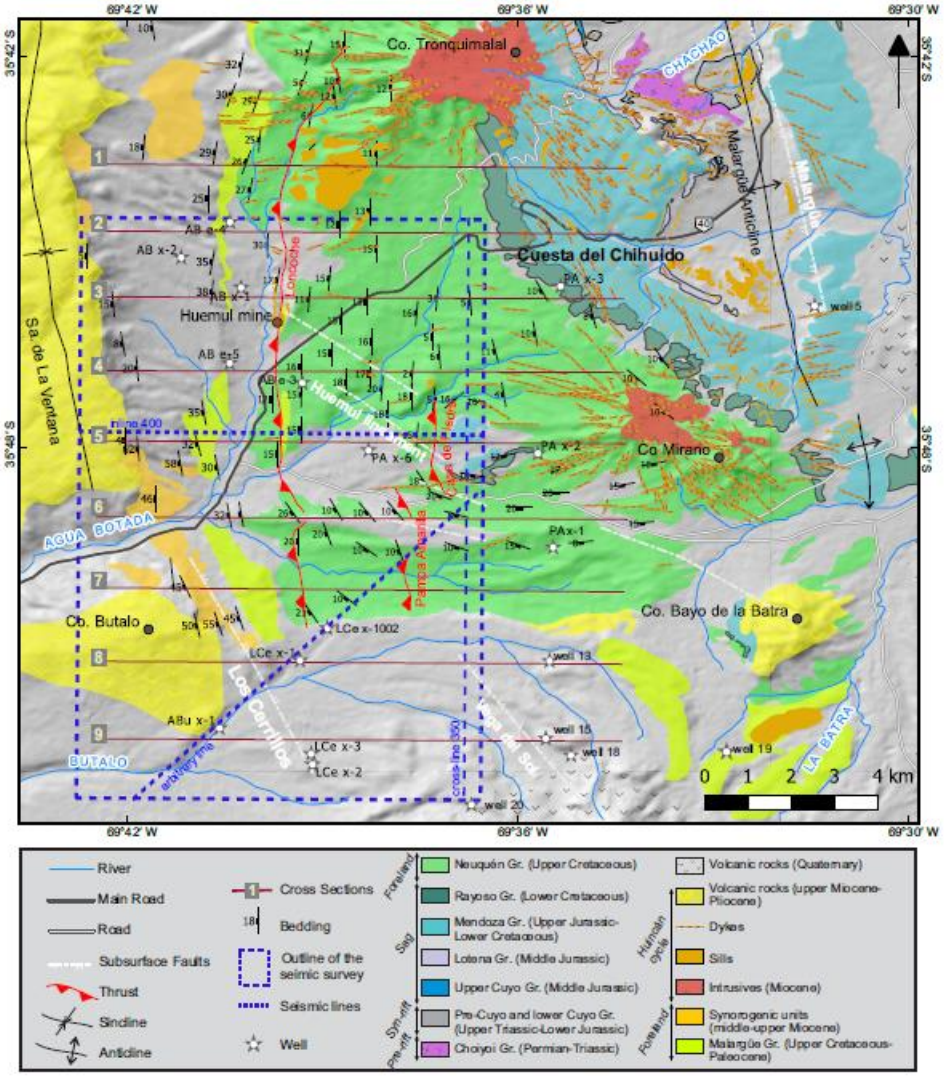

Figure 5: Main geologic units and structures in the Agua Botada area. Based on YPF, 1976; Nullo et al., 2005; Arcila Gallego, 2010 and own data.

The Loncoche fault (Figs. 5, 6) is a NS-trending and E-directed thrust developed in the Neuquén basin cover and probably detached along the Jurassic Auquilco Formation evaporites (Fig. 3). In the northern part of the study area (Fig. 6A), the Loncoche thrust folds the Upper Cretaceous Neuquén Group and the Neogene strata, including the approx. 10 Ma Loma Fiera deposits, in its hanging-wall. A sill intrudes a fault splay tapering towards the hinge of the fold (Fig. 6B). In the central zone (Fig. 6C), there is an old uranium mine site,

called Mina Huemul, associated with the Loncoche fault zone. Here we report a sheet intrusion, parallel to and in contact with the fault plane. There are secondary copper and uranium minerals precipitated as patinas as well as hydrocarbon traces in fault-parallel fractures, (Fig. 6D, E). In the southern area, the Loncoche fault cuts the Upper Cretaceous Neuquén Group strata (Fig. 6F); further south its displacement decreases and the Loncoche fault is no longer recognized in the field nor in the seismic data.

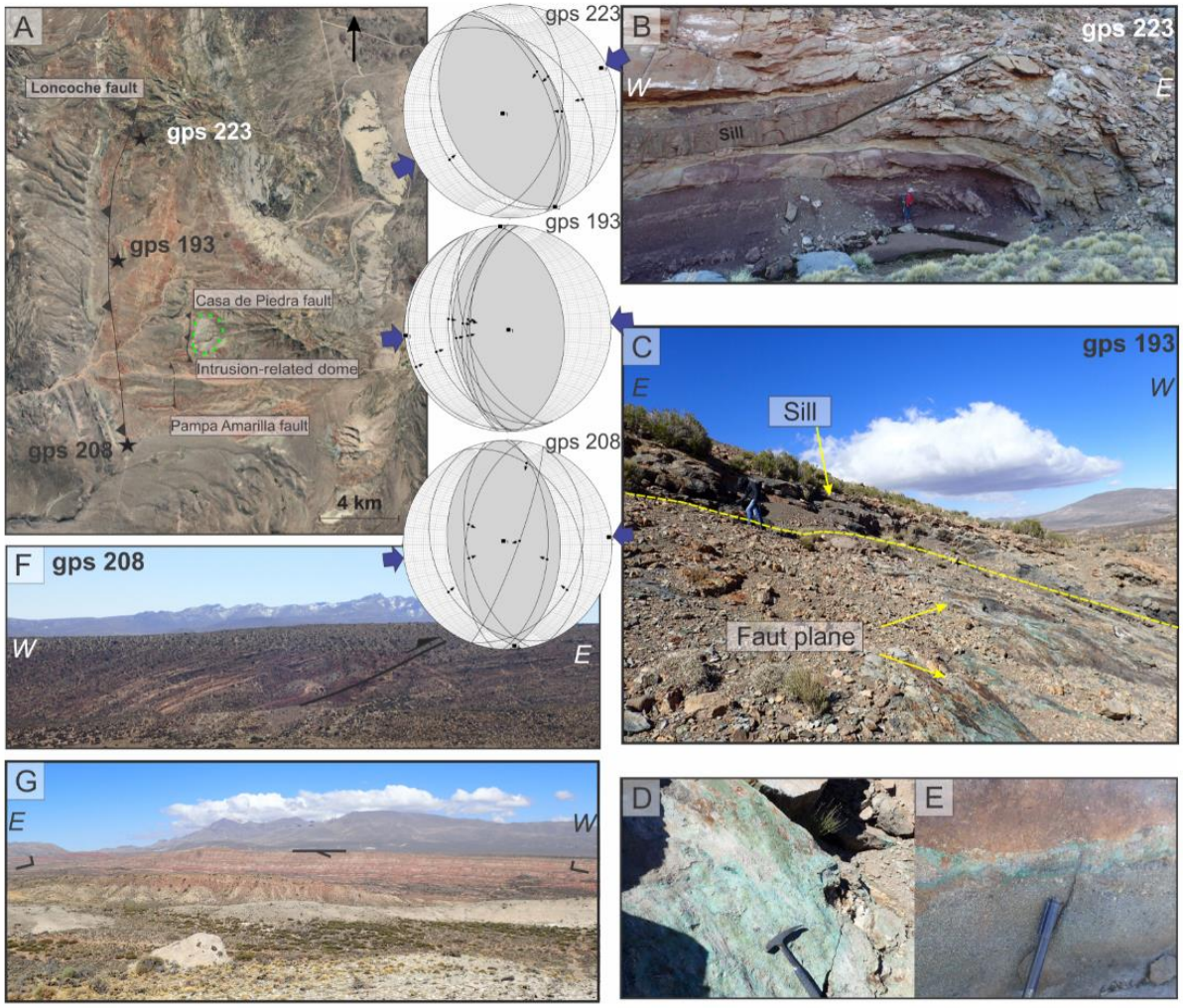

Figure 6: A) Aerial image with indication of the Loncoche, Casa de Piedra and Pampa Amarilla faults and the intrusion-related dome. Fault kinematic data displayed in equal area, lower hemisphere stereonets from stations 193, 208 and 223. The striae and sense of movement is represented by small arrows at the fault plane; the shortening axis is shown as blue arrows. B) Station gps 223 (35°43'23.20"S 69°39'9.84"W) where a sheet intrusion probably intrudes a fault splay developed in the

Neuquén Group rocks; an alternative is that the fault ramped up at the intrusion tip. C) Station gps 193 (35°45'57.95"S 69°39'38.11"W) near the uranium mine site. Notice a sill intruded concordantly to the fault plane where patinas of secondary minerals of copper and uranium cover the fractures. D) Detail of patinas and striae from Fig. 6C. E) Oil-impregnated sandstones of the Neuquén Group with secondary copper and uranium minerals (e.g. malachite, covellite, autunite). F) Station gps 208 (35°50'39.78"S 69°39'24.07"W), the Neuquén Group strata is tilted in the hanging-wall of the Loncoche fault. G) Photo (35°48'S 69°36'W) looking south from the core of the intrusion-related dome that probably causes the buttressing-related Casa de Piedra fault. Notice the radial dipping of the Neuquén Group redbeds and compare it with the dips plotted in the map (Fig. 5) that show the radial pattern.

The Casa de Piedra (YPF, 1976) and Pampa Amarilla faults are minor N-striking, E-directed thin-skinned structures recognized locally, with lengths <3 km (Figs. 5, 6). The Pampa Amarilla thrust is probably a splay of the Loncoche thrust that takes over part of the shortening lost by this structure in the south of the study area. The Casa de Piedra thrust is developed exclusively west of an intrusive body recognized in the seismic data (Figs. 7C, 8) and as a dome in the surface (Figs. 5, 6). We interpret that the fault is the result of buttressing against the intrusive (Figs. 7C, 8).

4.2 Subsurface structure

Interpretation of subsurface data (seismic and wells; Figs. 7, 8, 8 allowed us to determine the main structures at depth, linking them to surface geology.

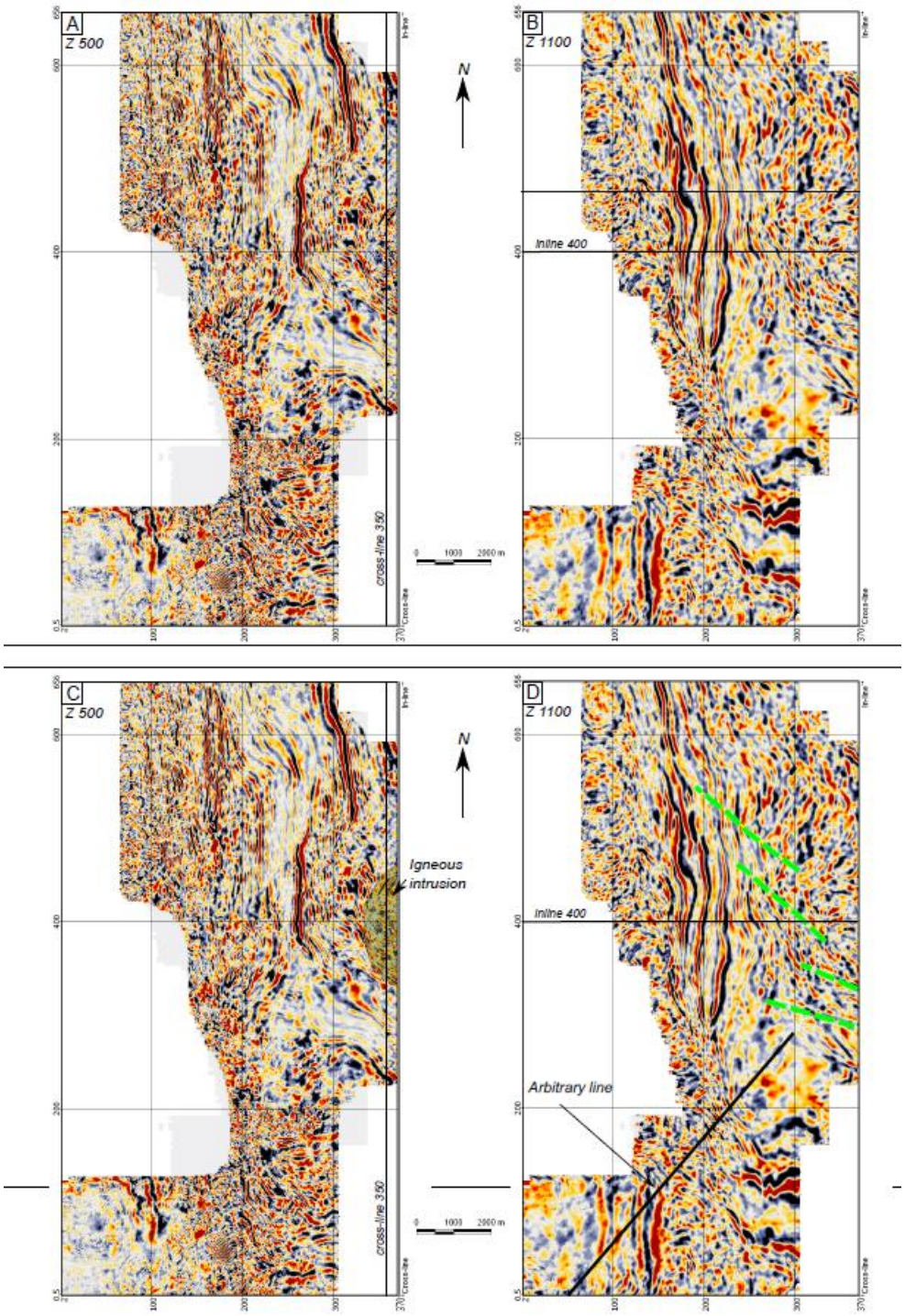

Figure 7: A) Uninterpreted time slice at z=500 ms. B) Uninterpreted time slice at z=1100 ms. C) Interpreted time slice at z=500 ms, the reflectors in the highlighted area are concentric to a high-noised core zone. This coincides in surface with the domed zone marked in the aerial image of Fig. 6A and the outcrops shown in Fig. 6G that we interpret as caused by an igneous intrusive in subsurface. D) Interpreted time slice at z=1100 ms, where a NW structure, called here Huemul

lineament and other oblique structures are shown. The cross-line and inline shown in Fig. 8 and the arbitrary line shown in Fig. 9 are marked.

The reverse, NNW-striking, west-verging Los Cerrillos fault (Fig. 8) was already recognized by Giambiagi et al. (2009) as an inverted normal fault, which forms part of the Palauco fault system (Fig. 2). It affects the basement and the Mesozoic deposits (Fig. 8), but it is covered by Quaternary deposits at surface. Wellbore data indicates that the Neuquén synrift basin stratigraphy shows important changes in thickness across the Los Cerrillos fault. In more detail, drill holes LCe x-1, LCe x-1002 and well 20 (Figs. 5, 8 and Table 1) ended in the Upper Triassic-Lower Jurassic Pre-Cuyo synrift deposits after more than 400 m (reaching 826 m in well 20) of these rocks, but immediately to the west the drill hole ABu x-1 (Table 1) ended in the Permian-Triassic Choiyoi Group which is overlain by ~200 m of the Pre-Cuyo rocks. The wedge geometry of synrift strata east of the Los Cerrillos fault (Fig. 8) suggests a half-graben controlled by this fault. We interpret that this fault was a synrift normal fault inverted during the Miocene. East of the Los Cerrillos fault, a minor blind structure, the Vega del Sol fault (Fig. 5), with similar attitude was recognized (YPF, 1995).

The subsurface expression of the Loncoche, Casa de Piedra and Pampa Amarilla faults could be determined from the seismic data. The Loncoche fault affects the Neuquén Group in the surface and the shales of the Mendoza Group in subsurface, probably detaching along the evaporites of the Auquilco Formation towards the west. It is composed of a principal fault and a series of minor splays with moderate angles. The Pampa Amarilla and Casa de Piedra thrusts are affecting the upper section of the Mendoza Group and are probably detached along the shales of the Vaca Muerta Formation, though this is not clearly recognized in the seismic data. The dome located east of the Casa de Piedra fault is observed in the seismic data (Fig. 8) due to the outward radial dipping of the reflectors and a high-noise core. The PA x-2 wellbore, located in the eastern part of the dome, between Cerro Mirano and the Casa de Piedra fault (Fig. 5) cuts through more than 170 m of andesites from a depth of 416 m to the end of hole. We interpret that intrusion (named here Pampa Amarilla intrusive)

produced doming of the Neuquén basin strata and that the Casa de Piedra fault is the result of buttressing against this rigid dome.

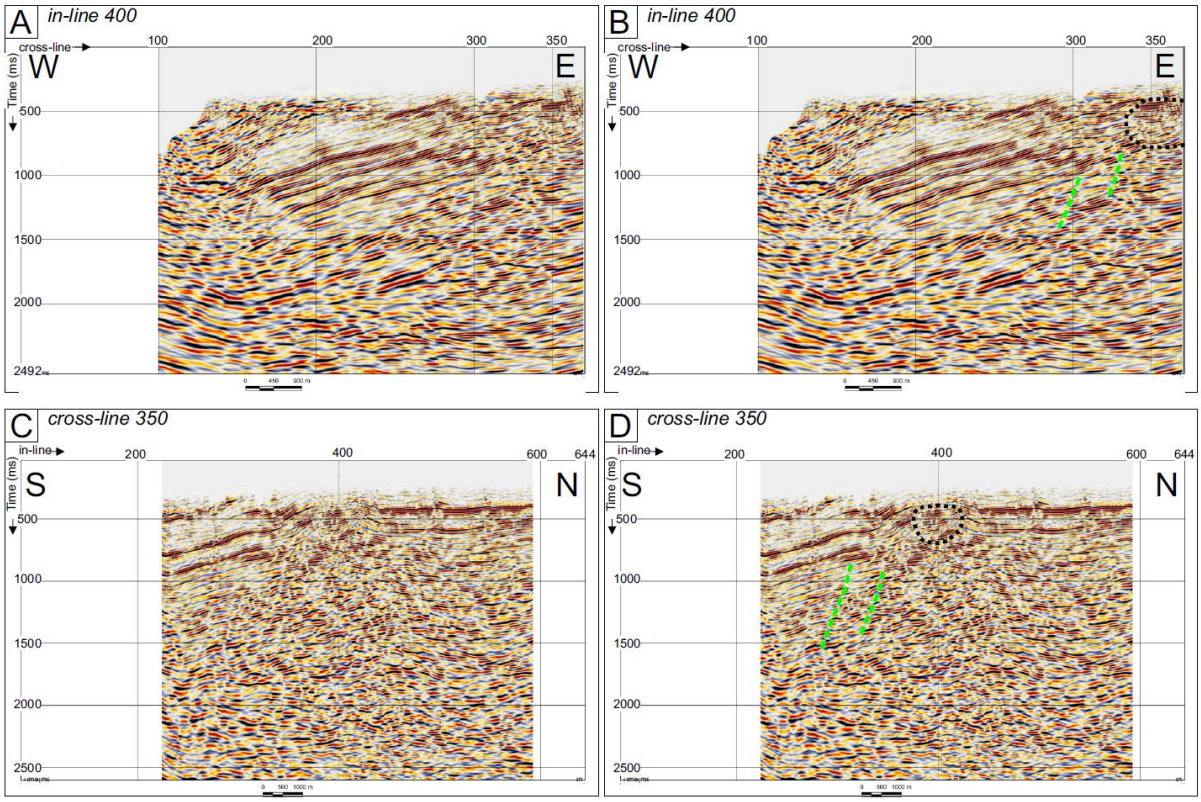

Figure 8

Figure 8: A) In-line 400 uninterpreted. B) In-line 400 showing the Huemul lineament (green dashed lines) and the intrusive (black dashed line). C) Cross-line 350 uninterpreted. D) Cross-line 350 showing the intrusive and the deformation it causes to the host rock. In green dashed lines the Huemul lineament is marked.

Time slices of the seismic data suggest that WNW- and NW-striking, subvertical structures are common in the northern sector of the study area, (Figs. 7, 8). The most important of these structures, named here Huemul lineament, is aligned with the Huemul mine and the Pampa Amarilla intrusive body (Figs. 5, 7).

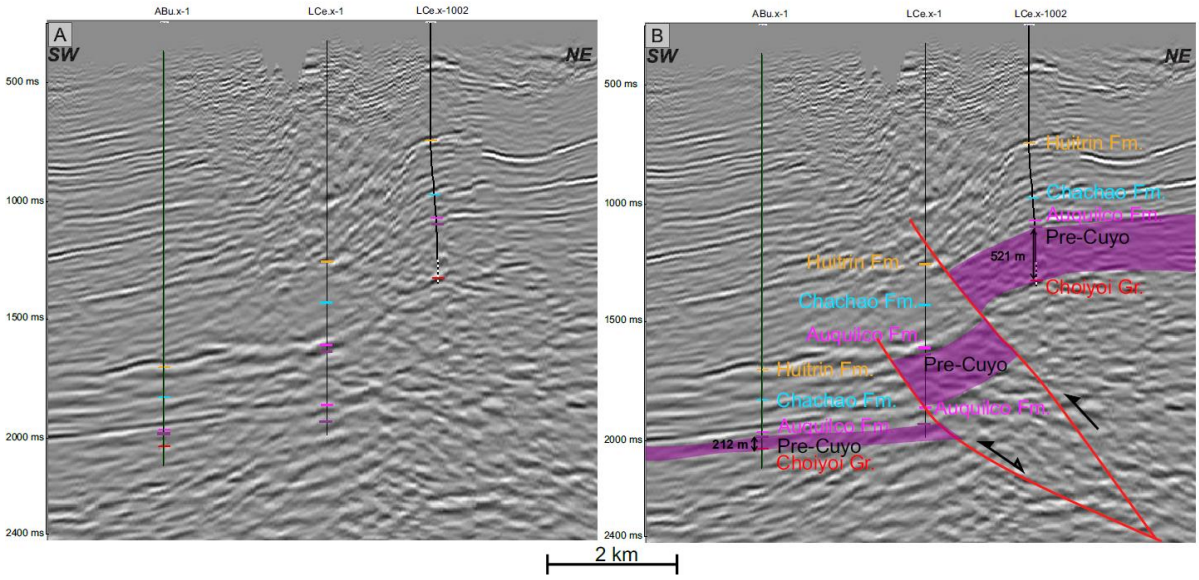

Figure 9: A) Uninterpreted arbitrary line oriented NE-SW (see map Fig. 5 and Fig 7D for location). B) Interpreted arbitrary line showing Los Cerrillos inverted normal fault that controlled the synrift thickness of Upper Triassic-Lower Jurassic Pre-Cuyo rocks. We interpret the uppermost fault as a hanging wall bypass.

Fm top depth	ABu.x-1	Fm top depth	LCe.x-1	Fm top depth	LCe.x-1002
922	Malargüe	1693	Huitrín	550	Rayoso
1160	Neuquén	1902	Agrio	659	Huitrín
2275	Huitrín	2191	Chachao	709	Agrio
2321	Agrio	2246	Vaca Muerta	1070	Chachao
2572	Vaca Muerta	2502	Auquilco	1112	Vaca Muerta
2888	Auquilco	2526	Pre-Cuyo	1296	Auquilco
2910	Pre-Cuyo	2944	Auquilco	1304	Lotena
3122	Choiyoi	3061	Pre-Cuyo	1330	Pre-Cuyo
3247	end of hole	3156	end of hole	1851	Choiyoi
				1901	end of hole
212	*thickness (m) of Pre-Cuyo*	*418*	*thickness (m) of Pre-Cuyo (minimum)*	*521*	*thickness (m) of Pre-Cuyo*

Table 1

Table 1: The stratigraphy cut through the drill-holes plotted in the arbitrary seismic line in Fig. 9 is shown with indication of the total apparent thickness of the Upper Triassic-Lower Jurassic Pre-Cuyo synrift deposits.

4.3 Pseudo-3D structural model

Nine W-E cross sections were constructed, separated by approx. 2 km each (Figs. 5, 9), by integrating dip data, unit contacts and surface fault traces with well log data and the interpretation of the 3D seismic cube. We reconstructed the initial geometry of the units and pre-existing normal faults (Fig. 9), and used kinematic forward-modelling to build sequential cross-sections taking into account Neogene sedimentation and isostatic changes using the flexural method in MOVE ©.

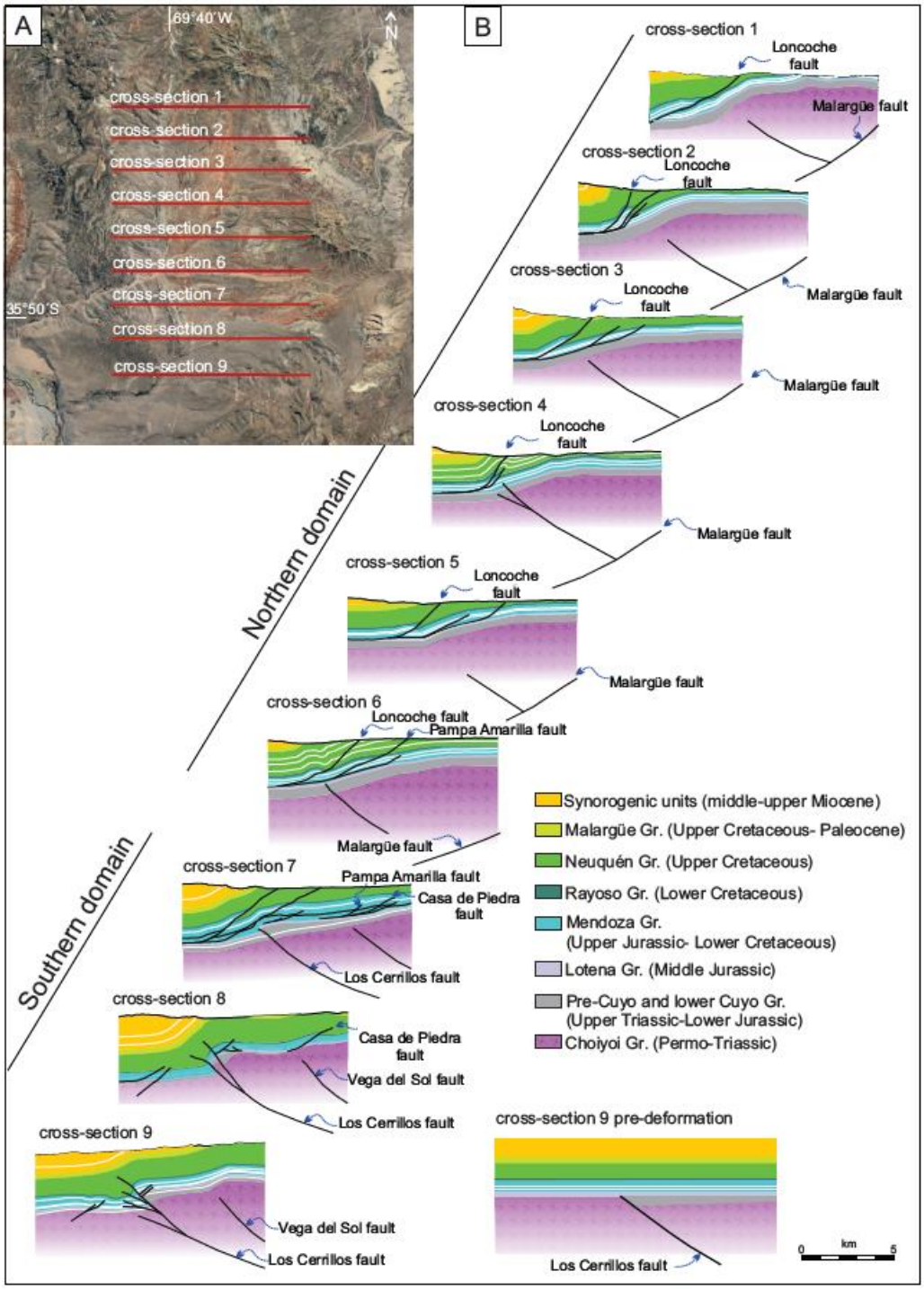

Figure 10: A) Google Earth image with location of W-E cross-sections in the Agua Botada area. B) Perspective view of the nine W-E cross-sections. The northern domain is characterized by the Malargüe anticline formed as consequence of reverse movement along the pre-existing Malargüe basement fault, and thin-skinned, east-directed thrusts. The southern domain is controlled by the

inversion of the Los Cerrillos fault. In the lowermost right corner the predeformation section is showed.

The cross-sections were extrapolated into a pseudo-3D structural model (Fig. 11). This ensures that the proposed structural model is consistent along strike. Structures and formation tops were mapped throughout the study area producing 3D surfaces that permit the characterization of the main structural features, such as main faults with lateral variations in displacement, depth to formation tops, bedding attitude, etc.

The northern domain (cross-sections 1 to 6, Fig. 9) is characterized by structures with eastern vergence. The thin-skinned Loncoche fault was modelled with a detachment level in the Upper Jurassic Auquilco evaporite. Two minor fault splays show variable geometries and displacement in the different cross-sections as constrained by wellbore, seismic and surface data. This fault system decreases its displacement southward and is absent south of cross-section 7 (Fig. 9). The deep seated Malargüe fault generates the Malargüe anticline in the north (sections 1-4) and also decreases its displacement towards the south. In our models, the high angle of the Loncoche fault is the result of tilting during folding related to the Malargüe fault.

The southern domain, in contrast, is characterized by a dominant western vergence (cross-sections 7 to 9, Fig. 9). The Los Cerrillos fault shows increasing complexity towards the south, with the development of fault splays, shortcut, bypass faults and minor backthrusts (Fig. 9). The Vega del Sol basement fault is recognized due to the anticline it forms in the Mesozoic cover. This fault increases its displacement towards the south.

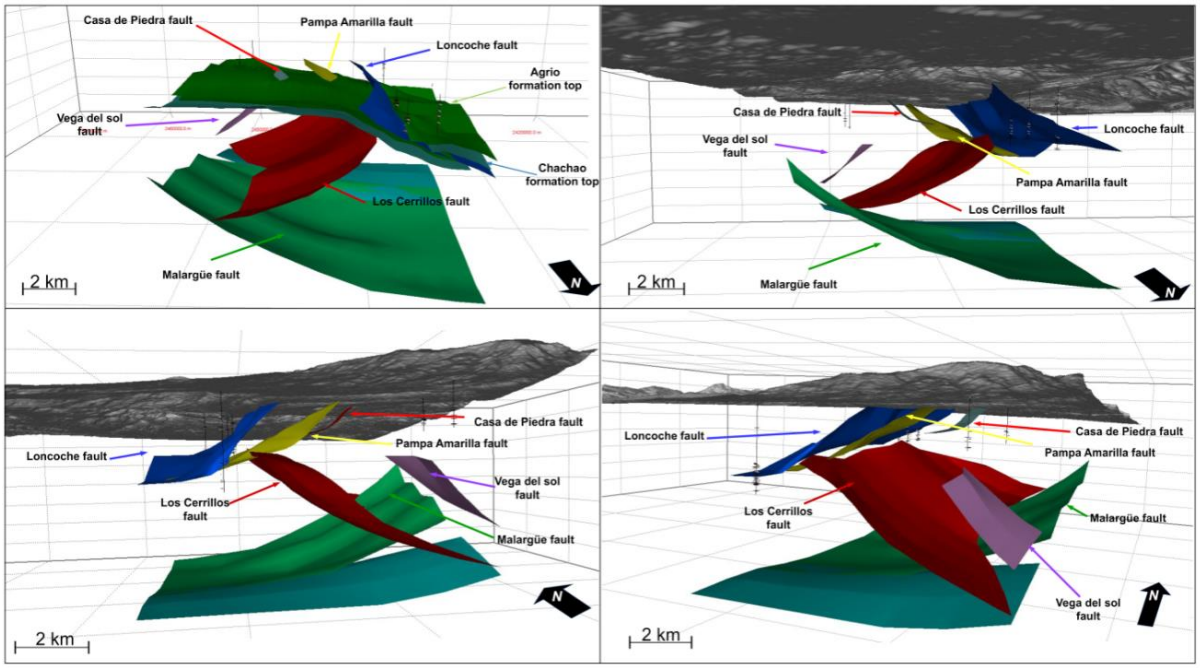

Figure 11: Different perspectives of the pseudo-3D model of the Agua Botada area. Upper green surfaces represent the top of the Chachao (dark green) and Agrio Formations (light green) of early Cretaceous age. Basement faults are the E-directed Malargüe fault, and W-directed Los Cerrillos and Vega del Sol faults. Thin-skinned E-directed faults are the Loncoche, Casa de Piedra and Pampa Amarilla faults.

4.4 Cenozoic intrusives and their relationship with structures

In order to study the relationship between the structural evolution of the Malargüe fold-and-thrust belt orogenic front and the Cenozoic igneous intrusions, we analyzed the spatial distribution of sills and dykes at the surface, from Google Earth satellite images, and at subsurface based on wellbore data. During fieldwork, we described the relationship of intrusions with the host rock and with structures (Fig. 12A), and measured kinematic indicators on mesoscale faults affecting the intrusions and their wallrocks. The relative timing of intrusion of sills and dykes is not always clear throughout the study area: some dykes

clearly post-date sills (e.g. Fig. 12B), while other dykes abut against sills (Fig. 12C). This latter could be the result of a pre-existing sill arresting the dyke or of synchronous emplacement with the dyke feeding the sill in the third dimension (Spacapan et al., 2016a). The similar composition of dykes and sills (Schiuma, 1994, Spacapan et al., 2016a, b) suggests that all belong to the middle Miocene to Pliocene Huincán magmatic cycle (Nullo et al., 2002). Our observations indicate that intrusions in the Agua Botada area are older than the Loma Fiera Formation (i.e. sills and dykes do not intrude this Formation), which has provided ages ~10 Ma (Baldauf, 1997; Horton et al., 2016), but intrude synorogenic beds from the Agua de la Piedra Formation (16-10 Ma, Silvestro and Atencio, 2009). This stratigraphical constraint indicates that sills and dykes were emplaced during the 16-10 Ma period, before the main phase of folding in the Malargüe anticline constrained to less than 7 Ma by Silvestro et al. (2005).

Most previous works focused on sills emplaced in the Vaca Muerta and Agrio Formations (Schiuma, 1994; Rodriguez Monreal et al., 2009; Spacapan et al., 2016a, 2018). In addition to these, we surveyed those emplaced in the red shales of the Rayoso and Neuquén Groups (Fig. 6). Our observations are mostly consistent with those reported in the referenced works. Most sills have sharp contacts with the wallrock, with borders subparallel to stratification of the wallrock (Fig. 12C). Most sill terminations are straight and abrupt (Fig. 12D), although wedge terminations were also observed (Fig. 6B). Sills are strongly controlled by rheological contrast, intruding shales but without affecting the more competent limestone, sandstone and conglomerate beds (Fig. 12B), as described in previous works (Spacapan et al., 2016a). The maximum observed thickness of sills is 70 m, while the maximum lengths reach 3000 m. Subvertical dykes with andesitic to basaltic andesite composition and porphyritic textures intrude all Mesozoic units. Most dykes radiate from two subvolcanic centers located in the Mirano and Tronquimalal peaks (Figs. 5, 12E, 12F). These two centers have an ellipsoidal shape, elongated along the WNW trend. The measurement of the orientation of 37 dykes from satellite images shows a predominant WNW trend, with ENE-, E- and NW-striking dykes also frequent (Fig. 13). Thickness and length are highly variable, but show a linear

relationship between both features and the dyke strikes. Dykes with ENE to WNW strikes are much longer and thicker than NW- to NE-striking dykes (Fig. 13).

To understand the relative timing between the Malargüe anticline and dyke and sill intrusion located at its backlimb, we unfolded and horizontalized the beds, taking the dykes as passive elements. By doing this, the dykes take a vertical to subvertical attitude (Fig. 13), suggesting that the intrusion occurred before the development of the anticline. This is consistent with the age constraints discussed at the beginning of this section.

We studied the available oil-well logs of the area (Fig. 5) to determine the intervals where igneous rocks were cut through. These rocks correspond to andesites of aphanitic to porphyritic texture with different alteration degrees and hydrocarbon traces. The apparent thickness reaches a maximum of 40 m and the thickest intervals are hosted in the shales of the Vaca Muerta Formation and the evaporites of the Auquilco Formation. We compared the thickness of igneous rocks in the drill-holes with the distance to the two volcanic centers identified, Tronquimalal and Mirano peaks (Supplementary Material). In the northern area (AB e-4, AB x-2, AB x-1, AB e-5; Fig. 5) there is a good correlation between the thickness of intrusives and the distance to the Tronquimalal neck, as well as in the central zone related to the Mirano neck; both necks show an associated swarm of dykes. In the southern area we did not recognize dykes outcropping in surface or necks, but there are some drill-holes (ABu x-1, LCe x-2 and well 18) that show high values of accumulated thickness of igneous rocks, such as the ABu x-1 accounting for more than 200 m (Supplementary Material). We interpret that this is probably related to subhorizontal intrusives, sills, which are covered by the Cenozoic deposits.

Observations at the Agua Botada area show that the Loncoche fault (Fig. 5) acted as a magmatic conduit allowing the emplacement of a sill that grades to an inclined sheet intrusion along the fault (Fig. 6). Furthermore, uranium and copper minerals precipitated along the contact of the sill and the fault, and the sill as well as the sandstones of the Neuquén Group wallrock are impregnated with hydrocarbons (Fig. 6E), indicating a link between reverse faulting, intrusion and fluid flow. On the other hand, subvertical strike-slip

faults locally control the emplacement of dykes, as already described by Spacapan (2016b). These dykes are heavily altered by hydrothermal fluids, with precipitation of fibers of hematite and calcite and hydrocarbon impregnation, which shows that fluid migration occurred during movement of these fractures. This suggests that the Loncoche reverse fault and the subvertical strike-slip faults have controlled magmatic emplacement and fluid and hydrocarbon migration. We will discuss this subject further in section 5.2.

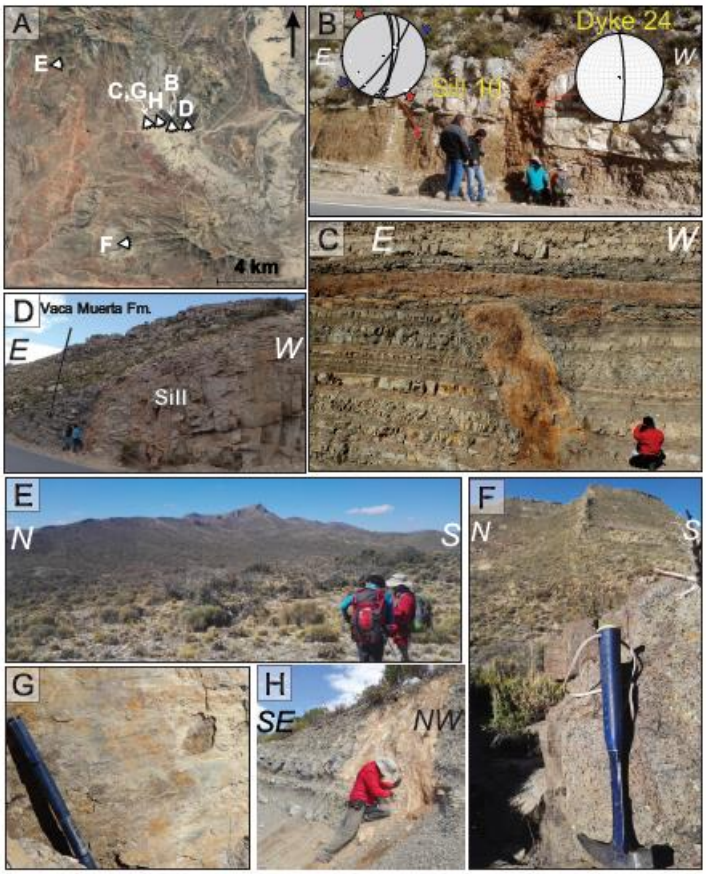

Figure 12

Figure 12: A) Aerial image (Google Earth) showing the location and orientation of the pictures described next. B) The dyke crosscuts a sill which is sheared with NNE dextral strike-slip faults subparallel to the dyke strike (GPS point AB dyke 24: 35°44'54.29"S 69°34'47.99"W). C) Dyke and sill intruding the Agrio Formation. The sill intrudes the pelitic layers of this unit due to low strength compared to the limestone beds. Apparently the dyke abuts against the sill (GPS point AB dyke 21:

35°44'55.48"S 69°35'16.80"W). This same outcrop was studied in detail by Spacapan et al. (2016a). D) Sharp contact between a sill and the Vaca Muerta Formation wallrock (GPS point AB sill 15 35°44'52.68"S 69°34'28.99"W). E) Photo looking eastward to the Mirano peak, the southernmost subvolcanic center, with radial dykes (GPS 35°48'S 69°36'W). F) Photo looking to the E pointing to the Tronquimalal peak with a dyke in the foreground which is radiated from the peak interpreted as subvolcanic center (GPS point AB dyke 34: 35°43'8.49"S 69°38'30.86"W). G) Subhorizontal striae and slip plane affecting a dyke, indicating strike-slip faulting (GPS point AB dyke 21: 35°44'55.48"S 69°35'16.80"W). H) Highly sheared and altered dyke intruding the Agrio Formation (GPS 35°45'1.19"S 69°34'53.89"W).

4.5. Kinematic analysis

Many intrusions in the Agua Botada area are affected by mesoscale faults with displacements less than 1 m. We measured fault slip data on 37 dykes and 22 sills and on Mesozoic rocks at 7 localities (Figs. 12, 13). A total of 87 fault plane-striation pairs with reliable sense of shear were measured. A dominant E- to ENE-directed shortening axis and subvertical extension axis is observed at sites close to the Loncoche fault (Fig. 6). In other sites, faults affect the interior of sills and dykes (Fig. 12G, H), as well as the contacts between dykes and wallrock. Overall, the NNE- to NE-trending faults show dextral movements, while the WNW- to NW-striking faults show sinistral movements (Fig. 13). Most data are consistent, indicating a strike-slip regime with E- to NE-directed shortening and N- to SE-directed extension.

An exception to this is the dextral movement of two of the NW-striking dykes (7 and 20 in Fig. 13) in the western flank of the Malargüe anticline, indicating a ENE-directed extension axis perpendicular to the trend of the anticline, and NNW-directed shortening axis. Here we propose that the ENE extension and NNW contraction may be due to local deviations of the contractional direction maybe related to previous structres, similar to what is observed nowadays from wellbore breakouts (Guzman et al., 2007). Other explanation is the dextral

movement of NW-striking faults preceded the intrusion of the dykes, as suggested by Spacapan et al. (2016).

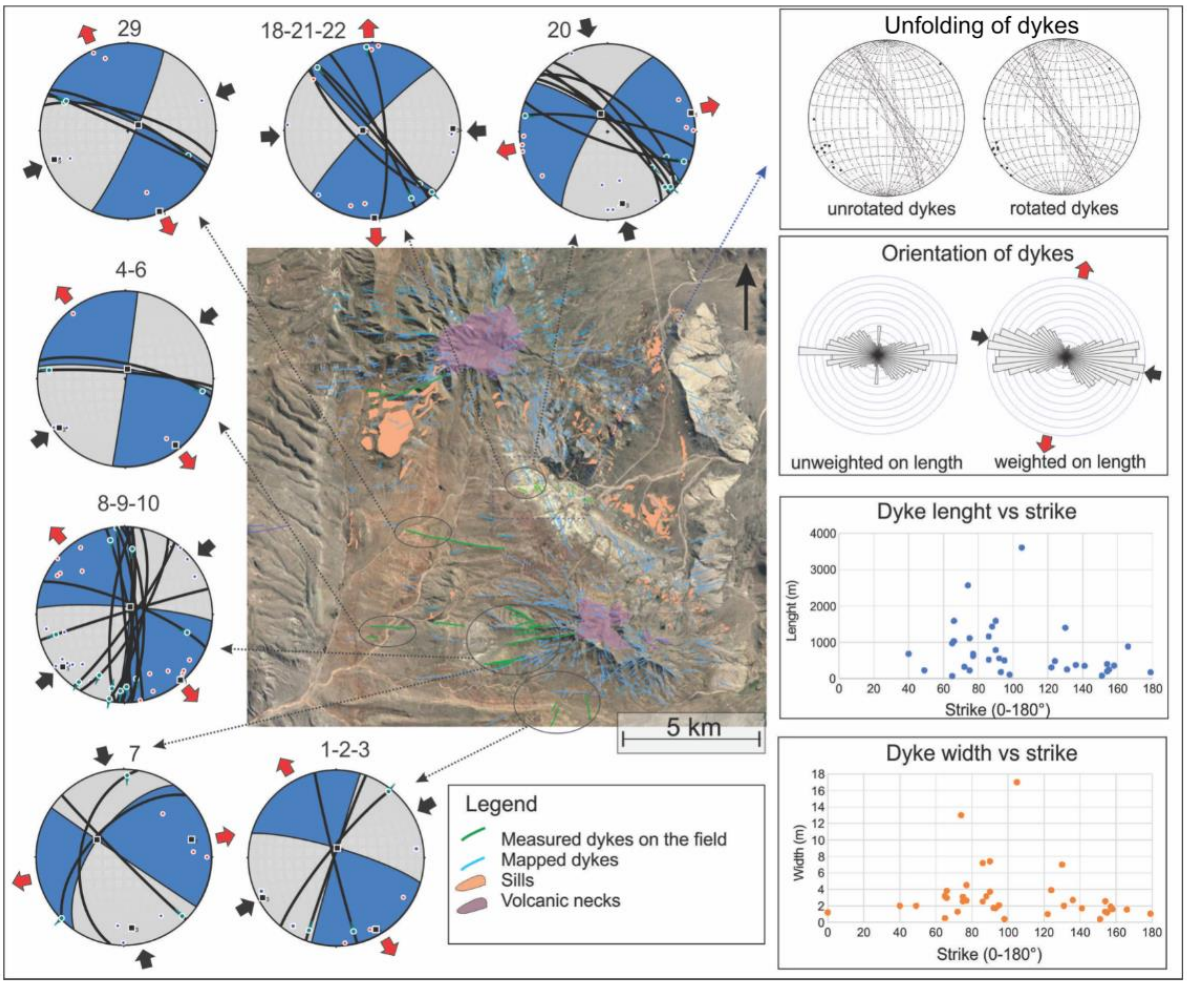

Figure 13

Figure 13: Kinematic data (green dots: striae data, blue dots: individual P-axes (contraction), red dots: individual T-axes (tension) obtained from the dykes in the area, showing that they are affected by strike-slip faulting. The unfolding performed in the dykes intruding the Mendoza Group in the backlimb of Malargüe anticline shows a better mechanical orientation when the data is restored to the horizontal position, indicating the dykes where intruded previous to the folding of Malargüe anticline, in agreement with geological data. The rose diagram includes both measured on field and mapped dykes, unweighted and weighted on length, showing a horizontal WNW oriented contraction (black arrows) and a NNE oriented extension (red arrows) at the time of intrusion. When compared the dyke length and width versus the strike, there is a correlation between the dimension of the intrusive and a

roughly W to WNW strike.

5. Discussion

5.1. Controls on intrusions

The geometry and connectivity of magmatic intrusions is the result of the combination of tectonic and magmatic processes and the lithology and pre-existing structures of the host rock (Magee et al., 2016). Tectonic processes include the influence of active structures during magma intrusion, that act as magma conduits (Kalakay et al., 2001; Galland et al., 2007 a, b; Ferré et al., 2012; Martínez et al., 2018; van Wyk de Vries and van Wyk de Vries, 2018) and the role of the stress field (Nakamura, 1977; Takada, 1989; Kavanagh, 2018). Magmatic processes refer to size, depth and shape of the magma source, magma injection rate, buoyancy and viscosity (Galland et al. 2007 a, b, 2018). Lithology controls the rheology of the host rock (Kavanagh et al., 2017; Galland et al., 2018) and pre-existing structures are weak zones that can also act as preferential pathways for magma (Ferré et al., 2012).

Dyke intrusion is strongly influenced by stress and crustal heterogeneities (Kavanagh, 2018). It is well established that the opening direction of dykes is perpendicular to the local minimum principal stress σ_3 (Anderson, 1951; Fossen, 2010; Kavanagh, 2018). This local stress is determined by the interaction of magma pressure and tectonic stress. In radial dyke systems emplaced under neutral stress conditions, magmatic pressure is similar in all direction and dykes of all orientations are similar in length. In contrast, radial dyke systems emplaced under a regional tectonic stress are elongated in the direction of the maximum horizontal stress σ_{Hmax} and dykes of the same orientation are more abundant than dykes of other trends (Odé, 1957; Nakamura, 1977). Pre-existing structures in the host rock are weak planes that can be used for magma migration and emplacement in dykes, depending on the orientations of fractures with respect to the tectonic stress and on magmatic overpressure (Delaney et al., 1986).

The emplacement of sills is the result of the interaction of tectonic stress and mechanical

layering of the host rock. Traditionally, opening perpendicular to σ_3 implying a vertical direction for the minimum stress has been proposed (Anderson, 1951; Hubbert and Willis, 1959). A recent review of sill complexes has shown that these are found in layered rocks under all stress regimes (Magee et al., 2016), which suggests that the presence of interfaces between rocks with different mechanical properties is the key factor (Galland et al., 2018). However, in some cases, sills have been documented in rocks with strong vertical mechanical discontinuities (bedding and foliation), where they were emplaced under local compressional conditions, which shows that the stress state controlled sill emplacement (Stephens et al., 2017). It seems that both mechanical layering of rocks and stress state can control sill emplacement, with one of these factors prevailing in some cases.

Magma supply for sills can be fed by a variety of structures, from dykes (Eide et al., 2016; Kavanagh et al., 2017) to inclined sheets connecting sills at different stratigraphic levels (Muirhead et al., 2012; Magee et al., 2016) to inclined sheets taking advantage of faults (Magee et al., 2013; Galland et al., 2007 a, b; Ferré et al., 2012).

Magmatic migration under contraction has been modeled by means of analogue modeling and compared with real examples in the Southern Central (Galland et al., 2007 a, b) and Northern Central Andes (Martínez et al., 2016; 2018) showing that thrusts and inverted faults could act as magma pathways even with considerably lateral migration in the shortening direction. In northern Chile basin inversion under Andean contraction is coeval with magma migration and this latter process influenced the geometry of the inverted faults and also the amount of shortening accommodate by the fault due to the role of igneous fluids as lubricants (Martínez et al., 2017; 2018). On the other hand these authors showed that magma migration, under shortening, is controlled by its viscosity; when higher the viscosity, the magma migrates shorter distances laterally and it is confined provoking uplift (Martínez et al., 2018).

In the study area, previous works have emphasized the role of layering and rheology of host rocks on sill intrusions, with intrusion favored in shale-dominated units and within these, in weak shale beds *vs.* strong sandstone beds (Spacapan et al., 2016a). Both within the study

area and throughout the Malargüe fold-and-thrust belt, it has been proposed that sills and laccoliths were fed by inclined sheet magma migration along thrusts (Araujo et al., 2013; Schiuma and Llambías, 2014), with thrusts acting as magma conduits and feeding sills in favorable stratigraphic intervals. No conclusive evidence of sill feeding by dykes has been reported in the area (Spacapan et al., 2016a). Our observations in the Loncoche fault support the role of active thrusts as magma conduits. Fault planes of the Loncoche fault are intruded by inclined sheets and mineral fibers on minor faults developed on the intrusions (Fig. 6) indicate fault movement once the inclined sheets were emplaced, showing that the fault was active during this period and not a pre-existing weakness. This is consistent with the age constraints for intrusions and activity of the Loncoche fault which suggest that both were coetaneous (see sections 4 and 5). On the other hand, the analysis of well data (section 4.4) suggests that sills were also fed by the intrusive centers of the Cerros Mirano and Tronquimalal, in which case some of the sills could be fed by these cylindrical intrusions. Dykes in the study area are radial systems developed from the magmatic centers of the Cerros Mirano and Tronquimalal, displaying a preferential E-W to ESE orientation, consistent with roughly E-W maximum horizontal stress σ_{Hmax} (Fig. 13), which indicates a control of the regional tectonic stress on their emplacement. Previous works have proposed that NW-trending pre-existing strike-slip faults controlled dyke intrusions (Spacapan et al., 2016b). We observed that some of the outcrop-scale faults are developed within the dykes indicating that strike-slip fault movement took place after intrusion (Fig. 13). Field observations alone do not allow us to determine if these faults moved shortly after dyke emplacement or if they are largely posterior. We will discuss this issue further in the following section.

5.2 Stress state during the magmatic intrusion and relation with fluid migration

Recent works have documented that the state of stress can be complex in orogenic fronts and depart from the expected compressional stress field, with the minimum principal stress σ_3 horizontal leading to the development of normal and strike-slip faults (Lacombe et al.,

2012; Tavani et al., 2015). Without neglecting other factors that influence the shape and mechanism of igneous intrusions, we propose that stress changes in the study area were an important factor determining the intrusion of dykes *vs.* sills.

The stress state and its changes in time in the study area are not well constrained. Guzmán et al. (2011) have studied the σ_{Hmax} directions in the Eocene to Oligocene from dyke trends, south of the study area, proposing a NE σ_{Hmax} for this period. During the Miocene, a change to E-W σ_{Hmax} took place and this remained until the present (Guzmán et al., 2007). The dominant contractional stress regime that led to crustal shortening and uplift of the Andes implies that $\sigma_{Hmax} = \sigma_1$, and the E-W direction was determined by the direction of plate convergence along the Argentina-Chile subduction zone (Pardo Casas and Molnar, 1987; Somoza, 1998; Norabuena et al., 1999). Local fluctuations to WNW or ESE σ_{Hmax} orientations have been suggested as the result of strain partitioning due to previous basement anisotropies (Branellec et al., 2015b) and topographic variations (Guzman et al., 2007; Mescua et al., 2014).

Our observations and previous works in nearby areas (Galland et al., 2007a, b; Araujo et al., 2013; Schiuma and Llambías, 2014) indicate that sill intrusions were fed by inclined sheets using thrusts as magmatic conduits. We documented continued activity of thrusts after magmatic intrusion at the Loncoche fault (Fig. 6). This suggests that sill intrusions took place in a compressive regime, where σ_1 was horizontal with E-W trend and the vertical minimum principal stress favoured horizontal fracture opening. This indicates that in the study area, both stress state and mechanical layering acted as main factors that conditioned sill intrusion.

The plan-view elongated shape of the radial dykes is the result of an E-W σ_{Hmax}, which is most likely the unchanged σ_1 determined by plate convergence. The NW- to WNW-striking dykes are emplaced in strike-slip faults, that may be pre-existing faults as suggested by Spacapan et al. (2016b); however, fault slip data from small scale faults affecting the contact between dykes and wallrock, as well as the interior of the dykes, indicate that faults were reactivated after intrusion. Mechanical analysis shows that subvertical faults display low slip

and dilation tendencies under horizontal compression, while in a vertical radial extension stress regime ($\sigma_2 = \sigma_3$), vertical fractures subparallel to σ_1 are likely to open, and vertical fractures oblique at low angles to σ_1 can open and shear (Stephens et al., 2017). This stress state has been indicated as one of the possible origins of the "σ_2 paradox" that produces strike-slip and normal faults in the frontal region of thrust wedges (Tavani et al., 2015) and can explain (i) the reactivation of pre-existing strike-slip faults with a dilation component to allow dyke emplacement, and (ii) the continued movement of the faults that produced small scale strike-slip faults. Field observations, as cross-cutting relationships between dykes and sills, similar composition, and that both are not intruding units younger than 10 Ma (Loma Fiera Fm.) suggest that dykes and sills were emplaced during the same time period (16-10 Ma, see section 4.4). We propose that during this period, the region was subjected to a stress regime with $\sigma_1 >> \sigma_2 \sim \sigma_3$. In this scenario, σ_2 and σ_3 could be interchanged producing alternating compression and strike-slip regimes (Zoback, 2010). Furthermore, this stress state has been recognized during the Pliocene-present in the orogenic front of the Malargüe fold-and-thrust belt (Mescua et al., in review), which suggests that the stress state in the region was constant since the early Miocene to the present in the study area.

The circulation of hydrothermal fluids and hydrocarbons in the faults of the study area is demonstrated by (i) copper and uranium mineralizations associated to the sill emplaced in the Loncoche fault; (ii) hydrothermal alteration in dykes that present strike-slip shearing with growth of hydrothermal mineral fibers; (iii) hydrocarbon impregnations in both kinds of structures. These observations imply that active thrusts and strike-slip faults, including major structures and outcrop-scale faults, acted as fluid carriers. Hydrothermal fluids migrated through these fault zones, leading to alteration of igneous intrusions and host rock and to the precipitation of mineralizations, locally with economic interest such as in the Huemul mine. Hydrocarbons also migrated through the faults. Strike-slip faults affect sills that are hydrocarbon reservoirs in many oilfields in the region (Comeron et al., 2002; Witte et al., 2012; Schiuma and Llambías, 2014; Spacapan et al., 2016, 2017), suggesting that the development of strike-slip faults can enhance fracture connectivity and be an important

factor in the migration of hydrocarbons into these reservoirs.

5.3 Tectonic and magmatic evolution of the study area

During the emplacement of dykes and sills, between 16 and 10 Ma, a foredeep area developed in the northern domain (Silvestro et al., 2005). The active structure during that period is interpreted by Silvestro et al. (2005) to be the Chacaico basement fault, located approx. 30 km toward the west (Fig. 4). Crosscutting relationships between dykes and sills, intruded during this period, indicate that they were synchronically emplaced. This suggests, a priori, that the magma intrusion was controlled by either a strike-slip/compression ($\sigma v=\sigma 2$ and $\sigma 2\sim\sigma 3$) or a compression/strike-slip ($\sigma v=\sigma 3$ and $\sigma 2\sim\sigma 3$) stress regime (Fig. 14A). We postulate that under this stress field regime pre-existing WNW- to E-striking structures were prone to dilate and were used as magma conduits.

After the deposition of the synorogenic deposits of the Loma Fiera Formation (approx 10 Ma, Fuentes et al., 2016), movement along the Doña Juana basement structure and associated thin-skinned thrusts and backthrusts generates the Sierra de la Ventana syncline (Fig. 4), as suggested by the lack of angular unconformities in the synorogenic units in the syncline and U/Th-He (AHe) thermochronological studies on apatite indicating a 8.9 to 7 Ma exhumation time for the Valenciana anticline (Bande et al., in press). During this period (10-7 Ma), a wedge-top depocenter is developed in the western sector of the Agua Botada area (Fig. 14B). The Loncoche fault represented the thrust front for that time. The eastward advance of the thrust system, suggest that the stress regime was a compressional one. This also correlates with the absence of dykes intruded during this period (10 -7 Ma) which may be influenced by this stress field. Under this stress field, at approx. 8 Ma, the Malargüe anticline started to develop, and continued its activity at least up to 1 Ma (Silvestro et al. 2005; Bande et al., in press). The Coyocho basalts (6.7-2.7 Ma) unconformably cover Cenozoic strata folded into the Sierra de la Ventana syncline, indicating the fossilization of the Loncoche fault after 7 Ma (Fig. 14C).

In the southern domain, during the first Miocene compressional period (16-10 Ma; Fig. 14D), active structures were localized in the inner sector of the Malargüe fold-and-thrust belt and in the Palauco fault system (Silvestro and Atencio, 2009). One of the faults of this system corresponds to the Los Cerrillos fault. Our model proposes that during this period and under a compressional stress regime, sills cut by the oil exploration wells were emplaced. The pre-existing Palauco system experienced a reactivation during the 11-8 Ma period (Fig. 14E) (Silvestro and Atencio, 2009) and during the last stage, since 7 Ma, the stress regime changed to a strike-slip one (Fig. 14F), as proposed by Mescua et al. (in review).

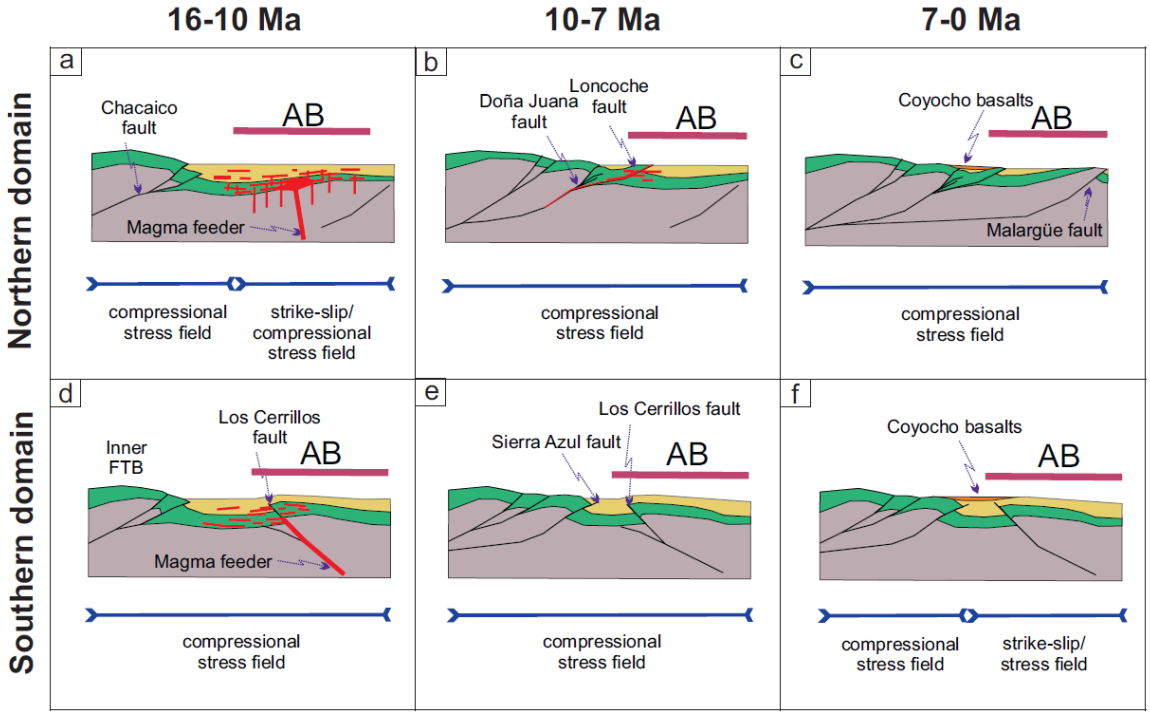

Figure 14

***Figure 14*:** Structural evolution of the northern (A-C) and southern (D-F) domains of the Agua Botada (AB) area. A) At the beginning of contraction in the Malargüe fold-and-thrust belt, the AB area was subjected to a strike-slip/compression stress regime. Under this regime, sills and dykes intruded the

Mesozoic beds and Neogene synorogenic strata of the Agua de la Piedra Formation. B) With the advance of the thrust front, at 10-7 Ma, the AB area was under compression, and few sills intruded the sedimentary sequences feeded from the active thrusts. C) The thrust front reached the Malargüe anticline area at approx 8-7 Ma. The western AB area was unconformably covered by the Coyocho basalts. D) In the southern domain, the thrust front was located at the Los Cerrillos fault, during the 16-10 Ma period. The AB area was under a compressional stress field, and sills intruded the Mesozoic units, feeded from the Los Cerrillos fault. E) During the 10-7 Ma period, the area was under compression, and the Sierra Azul fault developed. F) During the last stage, the stress field in the AB area changed to a strike-slip one, as documented by Mescua et al. (in review).

All these observations indicate that, in the study area: (i) sills are syn- or post-tectonic with respect to deformation of the western part of the study area, which started at 16 Ma (Silvestro and Atencio, 2009), (ii) sills and dykes were likely emplaced contemporaneously in the northern domain, with dykes emplaced shortly after sills and *vice versa*, but most intrusions predate the Loma Fiera Formation dated at 10 Ma; (iii) shearing of well-oriented dykes occurred before thin-skinned thrusting event (>10 Ma) under a strike-slip regime; (iv) the contraction and folding in the area, related to the Malargüe fault, took place after the main pulse of intrusion emplacement, coincident with the proposal of Silvestro and Atencio (2009) that indicates that the Malargüe anticline started to form at 7 Ma; and (V) there is no evidence of emplacement of dykes in the southern domain; instead, well logs indicate the presence of many igneous bodies, interpreted here as sills.

Taking into account that sill and dyke intrusion are favoured by the different stress fields acting in the region, this suggests that in the northern domain, between 16 and 10 Ma, the stress state fluctuated between compression/strike-slip and strike-slip/compression, in a way similar to that proposed at present for the orogenic front of the Malargüe fold-and-thrust belt to the north and south of the study area (Mescua et al., in review). This is in accordance with tensile joint analysis carried out by Branellec et al. (2015b) indicating a N-S subhorizontal

extensional direction during the pre-folding event. On the other hand, during that period, the southern domain was under pure compression and it is marked by the intrusion of sills.

6. Conclusions

Based on the structural characterization of dykes and sills in the framework of the evolution of the thrust front of the Malargüe fold-and-thrust belt, during the Miocene to Present, we infer the *in-situ* stress field acting at the time of intrusion. We propose that during the evolution of the thrust front, the local stress field changed from a compressional to a strike-slip/compressional one, favouring during this last stress field the synchronous emplacement of sills and dykes. We propose that the alternation of these stress regimes allowed hydrocarbon migration through thrusts and subvertical strike-slip faults as well. Previous NW-striking structures were not amenable to be inverted due to its high obliquity to the maximum principal stress in a compressional regime, but instead, they were prone to slip under a strike-slip/compressional regime; while WNW oriented previous structures were prone to dilate and acted as feeders from a magmatic source.

This interchange between both stress regimes is likely related to the similar values of the minimum (σ3) and intermediate principal stress (σ2) with an E-W oriented maximum principal stress (σ1) according to the plate convergence vector.

Acknowledgements

This research was supported by grants from the Agencia de Promoción Científica y Tecnológica (PICT-2015-1181 to J.F. Mescua and PICT-2016-0269 to L. Giambiagi). The authors want to thank Roch S.A. for providing the seismic and oil-well data. We would like to acknowledge the OpendTect 6.4.2 and MOVE2018.1 academic license to IANIGLA. This manuscript benefited from very helpful reviews by Olivier Galland and Fernando Martínez, and guest editors Olivier Lacombe and Pablo Granado.

References

Allmendinger, R. W., Cardozo, N., Fisher, D. M., 2012. Structural geology algorithms: Vectors and tensors. Cambridge University Press.

Anderson, E. M., 1951. The dynamics of faulting and dyke formation with applications to Britain. Hafner Pub. Co.

Araujo, V. S., Dimieri, L. V., Frisicale, M. C., Turienzo, M. M., Sánchez, N. P., 2013. Emplazamiento del cuerpo subvolcánico Laguna Amarga y su relación con las estructuras tectónicas andinas, sur de la provincia de Mendoza. Revista de la Asociación Geológica Argentina, 70(1), 40-52.

Arcila Gallego, P. A., 2010. Los depósitos sinorogénicos del sur de Mendoza y su relación con la faja plegada y corrida de Malargüe (35°-36° S), Mendoza. Argentina (Doctoral dissertation, Facultad de Ciencias Exactas y Naturales. Universidad de Buenos Aires).

Artabe, A. E., Morel, E. M., Spalletti, L. A., Brea, M., 1998. Paleoambientes sedimentarios y paleoflora asociada en el Triásico tardío de Malargüe, Mendoza. Revista Asociación Geológica Argentina, 53(4), 526-548.

Aydin, A., 2000. Fractures, faults, and hydrocarbon entrapment migration and flow. Marine and Petroleum Geology 17, 797-814.

Baldauf, P. E., 1997. Timing of the uplift of the Cordillera Principal, Mendoza Province, Argentina. M.S. thesis, George Washington University, p. 356.

Balgord, E. A., Carrapa, B., 2016. Basin evolution of Upper Cretaceous–Lower Cenozoic strata in the Malargüe fold- and- thrust belt: northern Neuquén Basin, Argentina. Basin Research, 28(2), 183-206.

Bande, A., Boll, A., Fuentes, F., Horton B., Stockli, D. F., (in press) Thermochronological constraints on the exhumation of the Malargüe fold-thrust belt, southern Central Andes. In: Opening and closure of the Neuquén Basin in the Southern Andes, Diego Kietzmann and Andrés Folguera (eds)

Barazangi, M. Isacks, B. L. Spatial distribution of earthquakes and subduction of the Nazca

plate beneath South America. *Geology* 4, 686–692 (1976).

Barton, C.A., Zoback, M.D. Moos, D., 1995. Fluid flow along potentially active faults in crystalline rock. Geology 23, 683-686.

Bechis, F., Cristallini, E. O., Giambiagi, L. B., Yagupsky, D. L., Guzmán, C. G., García, V. H., 2014. Transtensional tectonics induced by oblique reactivation of previous lithospheric anisotropies during the Late Triassic to Early Jurassic rifting in the Neuquén basin: insights from analog models. Journal of Geodynamics, 79, 1-17.

Bechis, F., Giambiagi, L. B., Tunik, M., Suriano, J., Mescua, J. F., Lanés, S., (in press) Tectono-stratigraphic evolution of the Atuel depocenter during the Late Triassic to Early Jurassic rift stage, Neuquén basin, west-central Argentina. In: Opening and closure of the Neuquén Basin in the Southern Andes, Diego Kietzmann and Andrés Folguera (eds)

Bermúdez, A., Delpino, D., 1989. La provincia basáltica andino cuyana (35°-37°LS). Revista de la Asociación Geológica Argentina, 44: 35-55.

Bermúdez, A., Delpino, D., Frey, F., Saal, A., 1993. Los basaltos de retroarco extraandinos. In Congreso Geológico Argentino (No. 12, pp. 161-172).

Bettini, F., 1982. Complejos efusivos terciarios presentes en las Hojas 30c y 32b (Puntilla del Huincán y Chos Malal), del sur de Mendoza y Norte del Neuquén, Argentina. In Actas V Congreso Latinoamericano de Geología 5: 79-114.

Boll, A., Alonso, A., Fuentes, F., Vergara, M., Laffitte, G., Villar, H. J., 2014. Factores controlantes de las acumulaciones de hidrocarburos en el sector norte de la cuenca Neuquina, entre los ríos Diamante y Salado, Provincia de Mendoza, Argentina. In IX Congreso de Exploración y Desarrollo de Hidrocarburos, Mendoza, Argentina, Actas (pp. 3-44).

Branellec, M., Callot, J. P., Aubourg, C., Nivière, B., Ringenbach, J. C. 2015a. Matrix deformation in a basement-involved fold-and-thrust-belt: a case study in the central Andes, Malargüe (Argentina). Tectonophysics, 658, 186-205.

Branellec, M., Callot, J. P., Nivière, B., Ringenbach, J. C., 2015b. The fracture network, a proxy for mesoscale deformation: constraints on layer parallel shortening history from the

Malargüe fold and thrust belt, Argentina. Tectonics, 34(4), 623-647.

Branellec, M., Nivière, B., Callot, J. P., Ringenbach, J. C., 2016. Mechanisms of basin contraction and reactivation in the basement-involved Malargüe fold-and-thrust belt, Central Andes (34–36 S). Geological Magazine, 153(5-6), 926-944.

Buchanan, A., Kietzmann, D., Palma, R., 2016. Evolución paleoambiental de la Formación Remoredo (Jurásico Inferior) en el depocentro Malargüe, Cuenca Neuquina Surmendocina. Revista de la Asociación Geológica Argentina, 74(2), 163-178.

Cobbold, P. R., Rossello, E. A., 2003. Aptian to recent compressional deformation, foothills of the Neuquén Basin, Argentina. Marine and Petroleum Geology, 20(5), 429-443.

Combina, A., Nullo, F., 2005. Tertiary volcanism and sedimentation in the southern Cordillera Principal, Mendoza, Argentina. In International Symposium on Andean Geodynamics (ISAG) 6:174-177.

Combina, A. M., Nullo, F., 2011. Ciclos tectónicos, volcánicos y sedimentarios del Cenozoico del sur de Mendoza-Argentina (35-37 S y 69 30'W). Andean Geology, 38(1), 198-218.

Comeron, R., González, J.M., Schiuma, M., 2002. Los Reservorios de las Rocas Ígneas Intrusivas. 5° Congreso de Exploración y Desarrollo de Hidrocarburos, IAPG, Rocas reservorio de las cuencas Productivas de la Argentina, p. 559-582, Mar del Plata, Argentina.

Cox, S.F., 2005. Coupling between deformation, fluid pressures, and fluid flow in ore-producing hydrothermal systems at depth in the crust. Economic Geology 100th Anniversary Volume, 39-75.

Delaney, P. T., Pollard, D. D., Ziony, J. I., McKee, E. H., 1986. Field relations between dikes and joints: Emplacement processes and paleostress analysis. Journal of Geophysical Research: Solid Earth, 91(B5), 4920-4938.

Dimieri, L. V. 1997). Tectonic wedge geometry at Bardas Blancas, southern Andes (36 S), Argentina. Journal of Structural Geology, 19(11), 1419-1422.

Donnadieu, F. Merle, O., 1998. Experiments on the indentation process during cryptodome intrusions: New insights into Mount St. Helens deformation. Geology, 26, 79–82.

Eide, C.H., Schofield, N., Jerram, D.A., Howell, J.A., 2016. Basin-scale architecture of deeply emplaced sill complexes: Jameson Land, East Greenland. Journal of the Geological Society, doi:10.1144/jgs2016-018.

Fennell, L. M., Folguera, A., Naipauer, M., Gianni, G., Rojas Vera, E. A., Bottesi, G., Ramos, V. A., 2017. Cretaceous deformation of the southern Central Andes: synorogenic growth strata in the Neuquén Group (35° 30′–37° S). Basin Research, 29, 51-72.

Ferré, E., Galland, O., Montanari, D., Kalakay, T., 2012, Granite magma migration and emplacement along thrusts: International Journal of Earth Sciences, p. 1-16.

Fossen, H., 2010, Structural geology, Cambridge University Press.

Franzese, J. R., Spalletti, L. A. 2001. Late Triassic–early Jurassic continental extension in southwestern Gondwana: tectonic segmentation and pre-break-up rifting. Journal of South American Earth Sciences, 14(3), 257-270.

Fuentes, F., Horton, B. K., Starck, D., Boll, A. 2016. Structure and tectonic evolution of hybrid thick-and thin-skinned systems in the Malargüe fold–thrust belt, Neuquén basin, Argentina. Geological Magazine, 153(5-6), 1066-1084.

Galland, O., Hallot, E., Cobbold, P.R., Ruffet, G., de Bremond d'Ars, J., 2007a. Volcanism in a compressional Andean setting: A structural and geochronological study of Tromen volcano (Neuquén province, Argentina). Tectonics, 26, TC4010, doi:10.1029/2006TC002011.

Galland, O., Cobbold, P. R., de Bremond d'Ars,J. Hallot, E., 2007b. Rise and emplacement of magma during horizontal shortening of the brittle crust: Insights from experimental modeling, J. Geophys. Res., 112, B06402, doi:10.1029/2006JB004604.

Galland, O., Bertelsen, H.S., Eide, C.H., Guldstrand, F., Haug, O.T., Leanza, H.A., Mair, K., Palma, O., Planke, S., Rabbel, O., ROgers, B., Schmiedel, T., Souche, A., Spacapan, J., 2018. Storage and transport of magma in the layered crust - Formation of sills and related flat-lying intrusions. In Buchardt, S. (ed.) Volcanic and Igneous Plumbing Systems, Elsevier: 113-138.

Giambiagi, L. B., Ramos, V. A., Godoy, E., Alvarez, P. P., Orts, S., 2003a. Cenozoic deformation and tectonic style of the Andes, between 33 and 34 south latitude. Tectonics,

22(4).

Giambiagi, L. B., Alvarez, P. P., Godoy, E., Ramos, V. A., 2003b. The control of pre-existing extensional structures on the evolution of the southern sector of the Aconcagua fold and thrust belt, southern Andes. Tectonophysics, 369(1-2), 1-19.

Giambiagi, L., Bechis, F., García, V., Clark, A. H., 2008. Temporal and spatial relationships of thick-and thin-skinned deformation: A case study from the Malargüe fold-and-thrust belt, southern Central Andes. Tectonophysics, 459(1-4), 123-139.

Giambiagi, L., Tunik, M., Barredo, S., Bechis, F., Ghiglione, M., Alvarez, P., Drosina, M. (2009a). Cinemática de apertura del sector norte de la cuenca Neuquina. Revista de la Asociación Geológica Argentina, 65(2), 278-292.

Giambiagi, L., Ghiglione, M., Cristallini, E., Bottesi, G. 2009b. Kinematic models of basement/cover interaction: Insights from the Malargüe fold and thrust belt, Mendoza, Argentina. Journal of Structural Geology, 31(12), 1443-1457.

Giambiagi, L., Tassara, A., Mescua, J., Tunik, M., Álvarez, P., Godoy, E., Greg, H., Pinto L., Spagnotto, S., Porras, H., Tapia, F., Jara, P., Bechis, F., García, V., Suriano, J. and Pagano, S., 2015. Evolution of shallow and deep structures along the maipo-tunuyán transect (33° 40´S): from the pacific coast to the andean foreland. En: Geodynamic Processes in the Andes of Central Chile and Argentina. Sepúlveda, S., Giambiagi, L., Moreiras, S.M., Pinto, L., Tunik, M., Hoke, G. y Farías, M. (Eds). Geological Society of London, Special Publication 399: 63-82.

Giampaoli, P., Dajczgewand, D., Dzelalija, F., 2002. La estructura del sector externo de la faja plegada y corrida de Malargüe a la latitud del río Salado, cuenca neuquina surmendocina, Argentina. In Congreso Geológico Argentino, 15, Actas (Vol. 3, pp. 168-173).

Granado, P., & Ruh, J. B. (2019). Numerical modelling of inversion tectonics in fold-and-thrust belts. Tectonophysics, 763, 14–29. https://doi.org/10.1016/j.tecto.2019.04.033

Groeber, P., 1946. Observaciones geológicas a lo largo del meridiano 70. Hoja Chos Malal. Revista de la Asociación Geológica Argentina. 1: 178-208.

Gulisano, C. A., 1981. El Ciclo Cuyano en el norte de Neuquén y sur de Mendoza. In

Congreso Geológico Argentino 8: 579-592.

Guzmán, C., Cristallini, E., Bottesi, G., 2007. Contemporary stress orientations in the Andean retroarc between 34 S and 39 S from borehole breakout analysis. Tectonics, 26(3).

Haney, M., Snieder, R., Sheiman, J. and Losh, S., 2005. A moving fluid pulse in a fault zone. Nature, 437, 46, doi:10.1038/437046a.

Hernando, I. R., Franzese, J. R., Llambias, E. J., Petrinovic, I. A., 2014. Vent distribution in the Quaternary Payún Matrú Volcanic Field, western Argentina: Its relation to tectonics and crustal structures. Tectonophysics, 622, 122-134.

Horton, B. K., Fuentes, F., Boll, A., Starck, D., Ramirez, S. G., Stockli, D. F., 2016. Andean stratigraphic record of the transition from backarc extension to orogenic shortening: A case study from the northern Neuquén Basin, Argentina. Journal of South American Earth Sciences, 71, 17-40.

Hubbert, M., Willis, D.G., 1957. Mechanics of hydraulic fracturing. Transactions of Society of Petroleum Engineers of AIME, 210, 153-163.

Kavanagh, J., 2018. Mechanisms of magma transport in the upper crust: dyking. In Buchardt, S. (ed.) Volcanic and Igneous Plumbing Systems, Elsevier: 55-88.

Kavanagh, J., Rogers, B.D., Boutelier, D., Cruden, A.R., 2017. Controls on sill and dyke-sill hybrid geometry and propagation in the crust: The role of fracture toughness. Tectonophysics 698: 109-120.

Kalakay, T. J., John, B. E., Lageson, D. R., 2001. Fault-controlled pluton emplacement in the Sevier fold-and-thrust belt of southern Montana, J. Struct. Geol., 23, 1151 – 1165.

Kleiman, L.E., Japas, M.S., 2009. The Choiyoi volcanic province at 34°S–36°S (San Rafael, Mendoza, Argentina): Implications for the Late Palaeozoic evolution of the southwestern margin of Gondwana. Tectonophysics, 437, 283-299.

Kozlowski, E., Manceda, R., Ramos, V.A., 1993, Estructura, In Ramos, V.A. (ed.) Geología y Recursos Naturales de Mendoza: 12 Congreso Geológico Argentino y 2 Congreso de Exploración de Hidrocarburos, Relatorio, p. 235–256.

Lacombe, O., Tavani, S., Soto, R., 2012. An introduction to the Tectonophysics special issue

"Into the deformation history of folded rocks". Tectonophysics 576–577, 1–3.

Legarreta, L., Gulisano, C., 1989. Análisis estratigráfico secuencial de la Cuenca Neuquina (Triásico Superior-Terciario Inferior, Argentina). In Simposio de Cuencas Sedimentarias Argentinas. Cuencas Sedimentarias Argentinas. In: 10 Congreso Geológico Argentino (Tucumán), Actas (p. 22).

Legarreta, L., Uliana, M. A., 1999. El Jurásico y Cretácico de la Cordillera Principal y la Cuenca Neuquina. Geología Argentina (Caminos, R.; editor). Servicio Geológico Minero Argentino, Anales, 29(16), 399-416.

Litvak, V. D., Spagnuolo, M. G., Folguera, A., Poma, S., Jones, R. E., Ramos, V. A., 2015. Late Cenozoic calc-alkaline volcanism over the Payenia shallow subduction zone, South-Central Andean back-arc (34° 30′–37° S), Argentina. Journal of South American Earth Sciences, 64, 365-380.

Llambías, E.J., Bertotto, G.W., Risso, C., Hernando, I., 2010. El volcanismo cuaternario en el retroarco de Payenia: una revisión. Revista de la Asociación Geológica Argentina, 67(2): 278-300.

Magee, C., Jackson, C.A., Schofield, N., 2013. The influence of normal fault geometry on igneous sill emplacement and morphology. Geology 41: 407-401.

Magee, C., Muihead, J., Karvelas, A., Holford, S., Jackson, C., Bastow, I, Schofield, N., Stevenson, C., McLean, C., McCarthy, W., Shtuckert, O., 2016. Lateral magma flow in mafic sill complexes. Geosphere, 12: 809-841.

Magee, C., Muirhead, J. D., Schofield, N., Walker, R. J., Galland, O., Holford, S. P., Spacapan, J. B., Jackson, C. A. L., McCarthy, W., 2018, Structural signatures of igneous sheet intrusion propagation: Journal of Structural Geology, https://doi.org/10.1016/j.jsg.2018.07.010.

Manceda, R., Figueroa, D., 1995. Inversion of the Mesozoic Neuquén rift in the Malargüe fold and thrust belt, Mendoza, Argentina. In: Tankard, A. J., Suárez, R., Welsink, H. (Eds.), Petroleum Basins of South America, American Association of Petroleum Geologists Memoir, 62 (1995), pp. 369-382.

Martínez, F., Bonini, M., Montanari, D., Corti, G., 2016. Tectonic inversion and magmatism in the Lautaro Basin, northern Chile, Central Andes: a comparative approach from field data and analog models. J. Geodyn. 94–95, 68–83.

Martínez, F., Montanari, D., Del Ventisette, C., Bonini, M., & Corti, G. ,2018. Basin inversion and magma migration and emplacement: Insights from basins of northern Chile. Journal of Structural Geology, 114(October 2017), 310–319. https://doi.org/10.1016/j.jsg.2017.12.008

Mathieu, L., van Wyk de Vries, B., Holohan, E.P., Troll, V.R., 2008. Dykes, cups, saucers and sills: Analogue experiments on magma intrusion into brittle rocks. Earth and Planetary Science Letters, 271, 1–13.

Mescua, J. F., Giambiagi, L. B., Ramos, V. A., 2013. Late Cretaceous Uplift in the Malargüe fold-and-thrust belt (35 S), southern Central Andes of Argentina and Chile. Andean Geology, 40(1).

Mescua, J. F., Giambiagi, L. B., Tassara, A., Gimenez, M., Ramos, V. A., 2014. Influence of pre-Andean history over Cenozoic foreland deformation: structural styles in the Malargüe fold-and-thrust belt at 35 S, Andes of Argentina. Geosphere, 10(3), 585-609.

Mosquera, A. Ramos, V.A. 2006. Intraplate deformation in the Neuquén Basin. En: Kay, S.M. & Ramos, V.A. (Eds.): Evolution of Andean margin: A tectonic and magmatic view from the Andes to the Neuquén Basin (35°–39° S latitude). Geological Society of America, Special Paper 407: 97-124.

Muirhead, J., Airoldi, G., Rowland, J., White, J., 2012. Interconnected sills and inclined sheet intrusions control shallow magma transport in the Ferrar large igneous province, Antarctica. Geol. Soc Am. Bull., 124: 162-180.

Nakamura, K., 1977. Volcanoes as possible indicators of tectonic stress orientation—principle and proposal. Journal of Volcanology and Geothermal Research, 2(1), 1-16.

Norabuena, E. O., Dixon, T. H., Stein, S., Harrison, C. G., 1999. Decelerating Nazca- South America and Nazca- Pacific plate motions. Geophysical Research Letters, 26(22), 3405-3408.

Nullo, F. E., Stephens, G. C., Otamendi, J., Baldauf, P. E., 2002. El volcanismo del Terciario

superior del sur de Mendoza. Revista de la Asociación Geológica Argentina, 57(2), 119-132.

Nullo, F. E., Stephens, G., Combina, A., Dimieri, L., Baldauf, P., Bouza, P., Zanettini, J. C. M., 2005. Hoja geológica 3569-III/3572-IV Malargüe, provincia de Mendoza. Servicio Geológico Minero Argentino. Instituto de Geología y Recursos Minerales.

Odé, H. 1957. Mechanical analysis of the dike pattern of the Spanish Peaks area, Colorado. Bull. Geol. Soc. Am., 68: 567-576.

Orts, D. L., Folguera, A., Giménez, M., Ramos, V. 2012. Variable structural controls through time in the Southern Central Andes (~ 36ºS). Andean Geology, 39(2), 220-241.

Pardo- Casas, F., Molnar, P., 1987. Relative motion of the Nazca (Farallon) and South American plates since Late Cretaceous time. Tectonics, 6(3), 233-248.

Ramos, V. A., Folguera, A., 2011. Payenia volcanic province in the Southern Andes: An appraisal of an exceptional Quaternary tectonic setting. Journal of Volcanology and geothermal Research, 201(1-4), 53-64.

Rodriguez Monreal, F., Villar, H. J., Baudino, R., Delpino, D., Zencich, S., 2009. Modeling an atypical petroleum system: A case study of hydrocarbon generation, migration and accumulation related to igneous intrusions in the Neuquen Basin, Argentina. Marine and Petroleum Geology, 26(4), 590-605.

Schiuma, M. F., 1994. Intrusivos del valle del Río Grande, provincia de Mendoza, su importancia como productores de hidrocarburos (Doctoral dissertation, Facultad de Ciencias Naturales y Museo).

Schiuma, M. F., Llambías E. J., 2014. Importancia de los Sills Como Reservorios en la Cuenca Neuquina del Sur de Mendoza. 9° Congreso de Exploración y Desarrollo de Hidrocarburos, IAPG, Trabajos Técnicos I, p. 331-349, Mendoza, Argentina

Seoane Borracer, F. N, Rocha, E., Armisen, M. R., Olivieri, G. A., Periale, S. L., Manceda, R. E. 2018. Proyecto exploratorio Pincheira, faja plegada y corrida de Malargüe, Cuenca Neuquina, provincia de Mendoza. In 10 Congreso de exploración y desarrollo de hidrocarburos, 75-90.

Silvestro, J., Atencio, M. 2009. La cuenca cenozoica del río Grande y Palauco: edad,

evolución y control estructural, faja plegada de Malargüe. Revista de la Asociación Geológica Argentina, 65(1), 154-169.

Silvestro, J., Kraemer, P., Achilli, F., Brinkworth, W. 2005. Evolución de las cuencas sinorogénicas de la Cordillera Principal entre 35-36 S, Malargüe. Revista de la Asociación Geológica argentina, 60(4), 627-643.

Somoza, R., 1998. Updated Nazca (Farallon)—South America relative motions during the last 40 My: implications for mountain building in the central Andean region. Journal of South American Earth Sciences, 11(3), 211-215.

Spacapan, J.B., Galland, O., Leanza, H., Planke, S., 2016a. Igneous sill and finger emplacement mechanism in shale-dominated formations: a field study at Cuesta del Chihuido, Neuquén Basin, Argentina. Journal of the Geological Society, doi.org/10.1144/jgs2016-056

Spacapan, J.B., Galland, O., Leanza, H. Planke, S., 2016b. Control of strike-slip fault on dyke emplacement and morphology. Journal of the Geological Society, 173, 573-576.

Spacapan, J. B., Palma, J. O., Galland, O., Manceda, R., Rocha, E., D'Odorico, A., Leanza, H. A., 2018. Thermal impact of igneous sill-complexes on organic-rich formations and implications for petroleum systems: A case study in the northern Neuquén Basin, Argentina. Marine and Petroleum Geology, 91, 519-531.

Spagnuolo, M. G., Litvak, V. D., Folguera, A., Bottesi, G., Ramos, V. A., 2012. Neogene magmatic expansion and mountain building processes in the southern Central Andes, 36–37 S, Argentina. Journal of Geodynamics, 53, 81-94.

Spalletti, L. A.,1997. Sistemas deposicionales fluvio-lacustres en el rift triásico de Malargüe (sur de Mendoza, República Argentina). In: Anales de la Academia Nacional de Ciencias Exactas, Físicas y Naturales, 49, 109-124.

Sruoga, P., Rubinstein, N. A., Etcheverría, M., Cegarra, M., 2009. Volcanismo neógeno y mineralización asociada, Cordillera Principal, Mendoza (35° S). In Congreso Geológico Chileno, 12, Actas, CD (Vol. 11, p. 4).

Stein, J. E., Ghiglione, M. C., Hlebszevitsch, J. C., 2018. Estructuras y entrampamientos

plio-pleistocenos (tardíos) en la plataforma deformada mendocina, Lindero de Piedra, Cuenca Neuquina In 10 Congreso de exploración y desarrollo de hidrocarburos, 111-123

Stephens, T.L., Walker, R.J., Healy, D., Bubeck, A., England, R.W., McCaffrey, K., 2017. Igneous sills record far-field and near-field stress interactions during volcano construction: Isle of Mull, Scotland. Earth and Planetary Science Letters 478: 159-174.

Takada, A., 1989. Magma transport and reservoir formation by a system of propagating cracks. Bulletin of Volcanology, 52(2), 118-126.

Tavani, S., Storti, F., Lacombe, O., Corradetti, A., Muñoz, J. A., Mazzoli, S., 2015. A review of deformation pattern templates in foreland basin systems and fold-and-thrust belts: Implications for the state of stress in the frontal regions of thrust wedges. Earth-Science Reviews, 141, 82-104.

Tunik, M., Folguera, A., Naipauer, M., Pimentel, M., Ramos, V. A., 2010. Early uplift and orogenic deformation in the Neuquén Basin: constraints on the Andean uplift from U–Pb and Hf isotopic data of detrital zircons. Tectonophysics, 489(1-4), 258-273.

Turienzo, M. M., 2010. Structural style of the Malargüe fold-and-thrust belt at the Diamante River area (34 30′–34 50′ S) and its linkage with the Cordillera Frontal, Andes of central Argentina. Journal of South American Earth Sciences, 29(3), 537-556.

Turienzo, M. M., Dimieri, L., Frisicale, C., Araujo, V. Sanchez, N., 2012. Cenozoic structural evolution of the Argentinean Andes at 34º40`S: A close relationship between thick and thin-skinned deformation. Andean Geology, 39(2), 317-357.

Uliana, M. A., Biddle, K. T., 1988. Mesozoic-Cenozoic paleogeographic and geodynamic evolution of southern South America. Revista Brasileira de geociencias, 18(2), 172-190.

Uliana, M. A., Legarreta, L., 1993. Hydrocarbons Habitat in a Triassic- To- Cretaceous Sub- Andean Setting: Neuquén Basin, Argentina. Journal of Petroleum Geology, 16(4), 397-420.

Uliana, M. A., Biddle, K. T., Cerdan, J., 1989. Mesozoic Extension and the Formation of Argentine Sedimentary Basins: Chapter 39: Analogs.

Uliana, M. A., Arteaga, M. E., Legarreta, L., Cerdán, J. J., Peroni, G. O., 1995. Inversion

structures and hydrocarbon occurrence in Argentina. Geological Society, London, Special Publications, 88(1), 211-233.

Valencio, D. A., Linares, E., Creer, K., 1969. Paleomagnetismo y edades geológicas de algunos basaltos terciarios y cuartarios de Mendoza y Neuquén. IVº Jornadas Geológicas Argentinas. Actas, 2, 397-415.

van Wyk de Vries, B., van Wyk de Vries, M., 2018. Tectonics and volcanic and igneous plumbing systems. In Buchardt, S. (ed.) Volcanic and Igneous Plumbing Systems, Elsevier: 167-189.

Vergani, G. D., Tankard, A. J., Belotti, H. J., Welsink, H. J., 1995. Tectonic evolution and paleogeography of the Neuquén Basin, Argentina. In: Tankard, A.J., Suárez, R, Welsink H. J. (Eds.): Petroleoum basins of South America. American Association of Petroleum Geologists, Memoir 62: 383-402.

Witte, J., Bonora, M., Carbone, C., Oncken, O., 2012. Fracture evolution in oil-producing sills of the Rio Grande Valley, northern Neuquén Basin, Argentina. AAPG bulletin, 96(7), 1253-1277.

Yagupsky, D. L., Cristallini, E. O., Fantín, J., Valcarce, G. Z., Bottesi, G., Varade, R. 2008. Oblique half-graben inversion of the Mesozoic Neuquén Rift in the Malargüe Fold and Thrust Belt, Mendoza, Argentina: New insights from analogue models. Journal of Structural Geology, 30(7), 839-853.

YPF. (1976). Unpublished internal report: Plano Geológico Zona Pampa Amarilla-Agua Botada.

YPF (1995). Unpublished internal report: Informe final de pozo NVS.x-1 Vega del Sol.

Zapata, T., Brissón, I., Dzelalija, F., 1999. The role of basement in the Andean fold and thrust belt of the Neuquén Basin. Thrust tectonics, 99, 122-124.

Zoback, M.D., 2010. Reservoir geomechanics. Cambridge University Press.

Figure captions

Figure 1: Location of the study area (white dashed rectangle) including the Agua Botada oil field (black continue polygon) and surroundings, with indication of the regional balanced cross-sections shown in Fig. 4. Base image is a LANDSAT7+ satellite image (RGB741 band combination).

Figure 2: A) Areal extension of the Neuquén basin (grey square shows the location of fig 2B). B) Map showing the master faults that bounded the Atuel, Río del Cobre, Valenciana, Malargüe, Palauco and Sierra Azul depocenters) of the Neuquén basin with indication of rift-related deposits (modified from Bechis et al., in press). C) Detailed map of the Valenciana (light blue area), Malargüe (pink area) and Palauco (green area) depocenters with the distribution of the Upper Triassic-Lower Jurassic synrift deposits and the main normal faults inferred from subsurface and surface data. The Agua Botada area corresponds to the blue dashed rectangle between Malargüe and Palauco depocenters (modified from Giambiagi et al., 2009a).

Figure 3: Stratigraphic chart showing the main tectonic phases of the Neuquén Basin and Malargüe fold-and-thrust belt (based on Giampaoli et al., 2002; Giambiagi et al., 2008; Mescua et al., 2014; Horton et al., 2016).

Figure 4: Regional balanced cross-sections, modified from Giambiagi et al. (2009b). See location in figure 1. The northern section cuts the Agua Botada northern domain. In this domain, the Malargüe fault (and fault-related anticline) is the main basement structure. The southern section crosses close to (~5 km) the Agua Botada southern domain, characterized by the inversion of a Triassic-Jurassic normal fault, the Palauco west-directed fault.

Figure 5: Main geologic units and structures in the Agua Botada area. Based on YPF, 1976; Nullo et al., 2005; Arcila Gallego, 2010 and own data.

Figure 6: A) Aerial image with indication of the Loncoche, Casa de Piedra and Pampa Amarilla faults and the intrusion-related dome. Fault kinematic data displayed in equal area, lower hemisphere stereonets from stations 193, 208 and 223. The striae and sense of movement is represented by small arrows at the fault plane; the shortening axis is shown as blue arrows. B) Station gps 223 (35°43'23.20"S 69°39'9.84"W) where a sheet intrusion probably intrudes a fault splay developed in the Neuquén Group rocks; an alternative is that the fault ramped up at the intrusion tip. C) Station gps 193 (35°45'57.95"S 69°39'38.11"W) near the uranium mine site. Notice a sill intruded concordantly to the fault plane where patinas of secondary minerals of copper and uranium cover the fractures. D) Detail of patinas and striae from Fig. 6C. E) Oil-impregnated sandstones of the Neuquén Group with secondary copper and uranium minerals (e.g. malachite, covellite, autunite). F) Station gps 208 (35°50'39.78"S 69°39'24.07"W), the Neuquén Group strata is tilted in the hanging-wall of the Loncoche fault. G) Photo (35°48’S 69°36’W) looking south from the core of the intrusion-related dome that probably causes the buttressing-related Casa de Piedra fault. Notice the radial dipping of the Neuquén Group redbeds and compare it with the dips plotted in the map (Fig. 5) that show the radial pattern.

Figure 7: A) Uninterpreted time slice at z=500 ms. B) Uninterpreted time slice at z=1100 ms. C) Interpreted time slice at z=500 ms, the reflectors in the highlighted area are concentric to a high-noised core zone. This coincides in surface with the domed zone marked in the aerial image of Fig. 6A and the outcrops shown in Fig. 6G that we interpret as caused by an igneous intrusive in subsurface. D) Interpreted time slice at z=1100 ms, where a NW structure, called here Huemul lineament and other oblique structures are shown. The cross-

line and inline shown in Fig. 8 and the arbitrary line shown in Fig. 9 are marked.

Figure 8: A) In-line 400 uninterpreted. B) In-line 400 showing the Huemul lineament (green dashed lines) and the intrusive (black dashed line). C) Cross-line 350 uninterpreted. D) Cross-line 350 showing the intrusive and the deformation it causes to the host rock. In green dashed lines the Huemul lineament is marked.

Figure 9: A) Uninterpreted arbitrary line oriented NE-SW (see map Fig. 5 and Fig 7D for location). B) Interpreted arbitrary line showing Los Cerrillos inverted normal fault that controlled the synrift thickness of Upper Triassic-Lower Jurassic Pre-Cuyo rocks. We interpret the uppermost fault as a hanging wall bypass.

Table 1: The stratigraphy cut through the drill-holes plotted in the arbitrary seismic line in Fig. 9 is shown with indication of the total apparent thickness of the Upper Triassic-Lower Jurassic Pre-Cuyo synrift deposits.

Figure 10: A) Google Earth image with location of W-E cross-sections in the Agua Botada area. B) Perspective view of the nine W-E cross-sections. The northern domain is characterized by the Malargüe anticline formed as consequence of reverse movement along the pre-existing Malargüe basement fault, and thin-skinned, east-directed thrusts. The southern domain is controlled by the inversion of the Los Cerrillos fault. In the lowermost right corner the predeformation section is showed.

Figure 11: Different perspectives of the pseudo-3D model of the Agua Botada area. Upper green surfaces represent the top of the Chachao (dark green) and Agrio Formations (light green) of early Cretaceous age. Basement faults are the E-directed Malargüe fault, and W-directed Los Cerrillos and Vega del Sol faults. Thin-skinned E-directed faults are the Loncoche, Casa de Piedra and Pampa Amarilla faults.

Figure 12: A) Aerial image (Google Earth) showing the location and orientation of the pictures described next. B) The dyke crosscuts a sill which is sheared with NNE dextral strike-slip faults subparallel to the dyke strike (GPS point AB dyke 24: 35°44'54.29"S 69°34'47.99"W). C) Dyke and sill intruding the Agrio Formation. The sill intrudes the pelitic layers of this unit due to low strength compared to the limestone beds. Apparently the dyke abuts against the sill (GPS point AB dyke 21: 35°44'55.48"S 69°35'16.80"W). This same outcrop was studied in detail by Spacapan et al. (2016a). D) Sharp contact between a sill and the Vaca Muerta Formation wallrock (GPS point AB sill 15 35°44'52.68"S 69°34'28.99"W). E) Photo looking eastward to the Mirano peak, the southernmost subvolcanic center, with radial dykes (GPS 35°48’S 69°36’W). F) Photo looking to the E pointing to the Tronquimalal peak with a dyke in the foreground which is radiated from the peak interpreted as subvolcanic center (GPS point AB dyke 34: 35°43'8.49"S 69°38'30.86"W). G) Subhorizontal striae and slip plane affecting a dyke, indicating strike-slip faulting (GPS point AB dyke 21: 35°44'55.48"S 69°35'16.80"W). H) Highly sheared and altered dyke intruding the Agrio Formation (GPS 35°45'1.19"S 69°34'53.89"W).

Figure 13: Kinematic data (green dots: striae data, blue dots: individual P-axes (contraction), red dots: individual T-axes (tension) obtained from the dykes in the area, showing that they are affected by strike-slip faulting. The unfolding performed in the dykes intruding the Mendoza Group in the backlimb of Malargüe anticline shows a better

mechanical orientation when the data is restored to the horizontal position, indicating the dykes where intruded previous to the folding of Malargüe anticline, in agreement with geological data. The rose diagram includes both measured on field and mapped dykes, unweighted and weighted on length, showing a horizontal WNW oriented contraction (black arrows) and a NNE oriented extension (red arrows) at the time of intrusion. When compared the dyke length and width versus the strike, there is a correlation between the dimension of the intrusive and a roughly W to WNW strike.

Figure 14: Structural evolution of the northern (A-C) and southern (D-F) domains of the Agua Botada (AB) area. A) At the beginning of contraction in the Malargüe fold-and-thrust belt, the AB area was subjected to a strike-slip/compression stress regime. Under this regime, sills and dykes intruded the Mesozoic beds and Neogene synorogenic strata of the Agua de la Piedra Formation. B) With the advance of the thrust front, at 10-7 Ma, the AB area was under compression, and few sills intruded the sedimentary sequences feeded from the active thrusts. C) The thrust front reached the Malargüe anticline area at approx 8-7 Ma. The western AB area was unconformably covered by the Coyocho basalts. D) In the southern domain, the thrust front was located at the Los Cerrillos fault, during the 16-10 Ma period. The AB area was under a compressional stress field, and sills intruded the Mesozoic units, feeded from the Los Cerrillos fault. E) During the 10-7 Ma period, the area was under compression, and the Sierra Azul fault developed. F) During the last stage, the stress field in the AB area changed to a strike-slip one, as documented by Mescua et al. (in review).